THE CALCULATION OF COMPRESSIBLE TRANSITIONAL, TURBULENT, AND RELAMINARIZATIONAL BOUNDARY LAYERS OVER SMOOTH AND ROUGH SURFACES USING AN EXTENDED MIXING-LENGTH HYPOTHESIS

B. K. Hodge and J. C. Adams
ARO, Inc., a Sverdrup Corporation Company

VON KARMAN GAS DYNAMICS FACILITY
ARNOLD ENGINEERING DEVELOPMENT CENTER
AIR FORCE SYSTEMS COMMAND
ARNOLD AIR FORCE STATION, TENNESSEE 37389

February 1978

Final Report for Period July 1974 — September 1977

Prepared for

This report has been reviewed by the Information Office (OI) and is releasable to the National Technical Information Service (NTIS). At NTIS, it will be available to the general public, including foreign nations.

APPROVAL STATEMENT

This report has been reviewed and approved.

ELTON R. THOMPSON
Project Manager, Research Division
Directorate of Test Engineering

Approved for publication:

FOR THE COMMANDER

MARION L. LASTER
Director of Test Engineering
Deputy for Operations

REPORT DOCUMENTATION PAGE		READ INSTRUCTIONS BEFORE COMPLETING FORM
1. REPORT NUMBER AEDC-TR-77-96	2. GOVT ACCESSION NO.	3. RECIPIENT'S CATALOG NUMBER
4. TITLE (and Subtitle) THE CALCULATION OF COMPRESSIBLE TRANSITIONAL, TURBULENT, AND RELAMINARIZATIONAL BOUNDARY LAYERS OVER SMOOTH AND ROUGH		5. TYPE OF REPORT & PERIOD COVERED Final Report, July 1974 – September 1977
		6. PERFORMING ORG. REPORT NUMBER
7. AUTHOR(s) B. K. Hodge and J. C. Adams, Jr., ARO, Inc.		8. CONTRACT OR GRANT NUMBER(s)
9. PERFORMING ORGANIZATION NAME AND ADDRESS Arnold Engineering Development Center Air Force Systems Command Arnold Air Force Station, TN 37389		10. PROGRAM ELEMENT, PROJECT, TASK AREA & WORK UNIT NUMBERS Program Element 65807F
11. CONTROLLING OFFICE NAME AND ADDRESS Arnold Engineering Development Center/DOTR Air Force Systems Command Arnold Air Force Station, TN 37389		12. REPORT DATE February 1978
		13. NUMBER OF PAGES 100
14. MONITORING AGENCY NAME & ADDRESS(if different from Controlling Office)		15. SECURITY CLASS. (of this report) UNCLASSIFIED
		15a. DECLASSIFICATION/DOWNGRADING SCHEDULE N/A

16. DISTRIBUTION STATEMENT (of this Report)

Approved for public release; distribution unlimited.

17. DISTRIBUTION STATEMENT (of the abstract entered in Block 20, if different from Report)

18. SUPPLEMENTARY NOTES

Available in DDC.

19. KEY WORDS (Continue on reverse side if necessary and identify by block number)

compressible flow	surface roughness
equations	boundary layer
turbulent boundary layer	transitions
models	
turbulence	

20. ABSTRACT (Continue on reverse side if necessary and identify by block number)

Numerical calculations based on the compressible boundary-layer equations and an integral form of the kinetic-energy-of-turbulence (IKET) equation are presented for a variety of conditions. The addition of the IKET equation permits the streamwise computation of an additional dependent variable normally taken as an empirical constant in conventional mixing-length formulations. A baseline turbulence model is developed and then modified to account for the

DD _{1 JAN 73} FORM 1473 EDITION OF 1 NOV 65 IS OBSOLETE

4.   TITLE (Continued)

SURFACES USING AN EXTENDED MIXING-LENGTH HYPOTHESIS

20.   ABSTRACT (Continued)

effects of favorable and adverse pressure gradients, roughness, and transpiration. Examples given include adverse and favorable pressure gradients, relaminarization, acoustic-energy-induced transition, surface roughness, and transpiration. The IKET-based extended mixing-length hypothesis is shown to be considerably more flexible than conventional mixing-length turbulence models.

AFSC
Arnold AFS Tenn

PREFACE

The work reported herein was conducted by the Arnold Engineering
Development Center (AEDC), Air Force Systems Command (AFSC), under
Program Element 65807F. The results of the research presented were
obtained by ARO, Inc. (a Sverdrup Corporation Company), operating
contractor for the AEDC, AFSC, Arnold Air Force Station, Tennessee,
under ARO Project Numbers V33P-04A, V33A-08A, and V33A-A8A. The manu-
script (ARO Control No. ARO-VKF-TR-77-62) was submitted for publica-
tion on September 29, 1977.

Portions of this report were presented by the authors in AIAA Paper
No. 77-682, entitled "The Calculation of Compressible, Transitional,
Turbulent, and Relaminarizational Boundary Layers over Smooth and Rough
Surfaces Using an Extended Mixing-Length Hypothesis," given at the AIAA
10th Fluid and Plasma Dynamics Conference, Albuquerque, New Mexico, June
27-29, 1977.

CONTENTS

ILLUSTRATIONS

TABLES

TABLES

APPENDIX

1.0 INTRODUCTION

During the past few years many different analysis techniques for turbulent boundary-layer flows have been developed and validated. While the computational aspects of these developments must not be disregarded, the real key to the understanding of how to properly analyze complex turbulent boundary-layer flows involves advances in turbulent transport modeling. Reviews of many of the various proposed mathematical models of turbulence may be found in Refs. 1 through 6, and the recent books by White (Ref. 7) and Cebeci and Smith (Ref. 8) give overall coverage of turbulent boundary-layer analysis methods, both old and new.

This report documents another turbulent boundary-layer analysis technique. The extended mixing-length hypothesis is first developed; then a baseline turbulence model is explored and the baseline model is modified to account for effects such as pressure gradients and roughness. The method is assessed by comparing computed results with experimental data for many different two-dimensional and axisymmetric turbulent boundary-layer flows, both incompressible and compressible.

2.0 ANALYTICAL CONSIDERATIONS

Many recently developed computational methods for turbulent boundary-layer flows utilize the "eddy viscosity" concept of Boussinesq and apply Prandtl's mixing-length hypothesis to correlate the turbulent shear stress as a function of the local mean flow field in the boundary layer. The recent compendium by Bushnell, Cary, and Harris (Ref. 9) provides a list of such programs. The method of Patankar and Spalding (Ref. 10), one of the better known and more widely documented codes, correlates the mixing length in terms of the local boundary-layer thickness with the correlation function as determined from flat-plate flows assumed applicable to general flow situations. One drawback is that the flat-plate correlation represents a reasonable approximation only for flows

7

with moderate pressure gradients and is not necessarily applicable for flows with large pressure gradients, either favorable or adverse. Drawing a direct relationship between the mixing length and the <u>local</u> mean flow preempts explicit consideration of the development of the turbulent field, and such methods are not very successful in predicting highly "nonequilibrium" flows such as relaminarization.

The present analysis utilizes an <u>i</u>ntegral form of the <u>k</u>inetic-<u>e</u>nergy-of-<u>t</u>urbulence (IKET) equation in which the mixing length is no longer directly correlated to the local flow parameters but is instead calculated. The additional equation thus allows the "history" of the turbulent state to be considered explicitly and the mixing-length correlation to vary as the turbulent boundary layer develops. This so called extended mixing-length approach is not new, having been developed by McDonald and Camarata (Ref. 11) and applied by McDonald and Fish (Ref. 12), Shamroth and McDonald (Ref. 13), McDonald and Kreskovsky (Ref. 14), and Chan (Refs. 15 through 17). The present work represents an extension of the same approach with emphasis on compressible flows. This method is similar to the approach of Bradshaw, Ferriss, and Atwell (Ref. 18) with the exception that use of the IKET equation eliminates the pressure-velocity diffusion process and necessitates an assumption as to the distribution of mixing length across the boundary layer.

The IKET method as presented in this report lies between the conventional mixing length and the one-equation hydrodynamic model of turbulence, to use the hierarchy of Launder and Spalding (Ref. 1).

2.1 GOVERNING EQUATIONS

The present analysis employs the compressible, time-averaged boundary-layer equations for two-dimensional or axisymmetric geometries as derived by Vaglio-Laurin (Ref. 19). As shown in the sketch, the body surface is defined by $y = 0$, and x is defined as along the body surface.

For axisymmetric bodies, $r(x)$ is the radius at x and y = 0. The velocity components are taken to be $\bar{u}$ and $\bar{v}$ in the x- and y- directions, respectively.
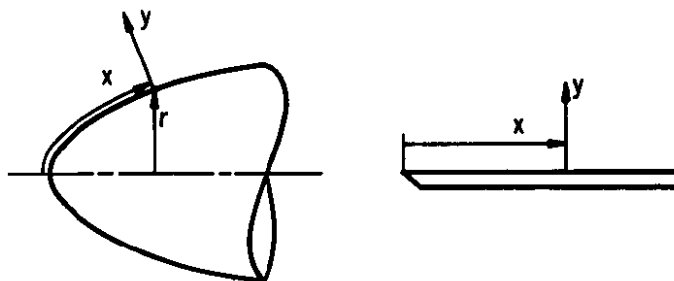
The governing equations of motion are as follows (see Nomenclature for terminology):

Continuity:

$$\partial/\partial x \; (\bar{\rho}\, \bar{u}\, r^j) + \partial/\partial y \; (\bar{\rho}\, V\, r^j) = 0 \tag{1}$$

Streamwise (x) Momentum:

$$\bar{\rho}\, \bar{u}\, \frac{\partial \bar{u}}{\partial x} + \bar{\rho}\, V\, \frac{\partial \bar{u}}{\partial y} = -\frac{d\bar{p}}{dx} - \left[1/2\, \bar{\rho}\, \bar{u}^2\, C_{D_r}\, \frac{D_r}{\ell_r^2}\right]^* + \frac{\partial}{\partial y}\left[\bar{\mu}\, \frac{\partial \bar{u}}{\partial y} - \bar{\rho}\, \overline{u'v'}\right] \tag{2}$$

Normal Momentum:

$$\partial \bar{p}/\partial y = 0 \tag{3}$$

Energy:

$$\bar{\rho}\, \bar{u}\, \frac{\partial \bar{h}}{\partial x} + \bar{\rho}\, V\, \frac{\partial \bar{h}}{\partial y} = \bar{u}\, \frac{\partial \bar{p}}{\partial x} + \bar{\mu}\, \left[\left(\frac{\partial \bar{u}}{\partial y}\right)^2\right]$$
$$- \bar{\rho}\, \overline{u'v'}\, \frac{\partial \bar{u}}{\partial y} + \frac{\partial}{\partial y}\left[\frac{\bar{\mu}}{Pr}\, \frac{\partial \bar{h}}{\partial y} - \bar{\rho}\, \overline{v'h'}\right] \tag{4}$$

with j = 1 for axisymmetric flow and j = 0 for planar (or two-dimensional) flow and with

$$V = \bar{v} + \frac{\overline{\rho' v'}}{\bar{\rho}} \tag{5}$$

_____

*An additional term for wall roughness, explained in Section 2.4.

The usual expressions for the mean and fluctuating parts of the depen-
dent variables are used; e.g.,

$$u = \bar{u} + u' \qquad (6)$$

Implicit in Vaglio-Laurin's derivation of the above equations are the
following stipulations:

a. The rates of change of the mean flow properties in the x
    direction $[\mathcal{O}(1)]$ are smaller than the rates of change in
    the y direction $[\mathcal{O}(\delta^{-1})]$ by an order of magnitude.

b. Mean squares and products of the turbulent fluctuations are
    $\mathcal{O}(\delta)$; that is, the turbulent level is small. The terms
    involving mean squares of the velocity fluctuations are
    taken to be negligible, which is valid for high Reynolds
    number flows with zero or favorable pressure gradients.

c. The time-averaged molecular transport quantities are approxi-
    mated by those pertaining to the mean flow properties; indeed,
    even the latter are negligible, except very near the wall,
    when compared with terms involving the turbulent transport
    quantities.

If subscript w denotes the wall and subscript e denotes the outer
edge of the boundary layer, the associated boundary conditions on the
aforementioned equations are

$$y = 0: \quad \bar{u} = \overline{u'v'} = \overline{\rho'v'} = \overline{v'h'} = 0$$

$$\bar{h} = \bar{h}_w \text{ (prescribed wall enthalphy)}$$

$$\frac{\partial \bar{h}}{\partial y} = 0 \text{ (adiabatic wall)} \qquad (7)$$

$$\bar{v} = 0; \quad \bar{v}\,\bar{\rho} = (\bar{v}\,\bar{\rho})_w \text{ (transpiration)}$$

$$\lim y \to \infty: \quad \overline{v'h'} = \overline{u'v'} = \overline{\rho'v'} = 0 \tag{8}$$

$$\overline{u} \longrightarrow U_e$$

$$\overline{h} \longrightarrow h_e$$

which reflects the no-slip condition at the wall as well as a prescribed wall enthalphy (or temperature) or an adiabatic wall. The normal momentum equation Eq. (3)] implies that the static pressure variation across the boundary layer is negligible and that the static pressure distribution, $\overline{p}(x)$, is an external imput to the boundary-layer analysis from a separate inviscid analysis or from experimental data. The outer-edge velocity, U_e, as well as the outer-edge enthalpy, h_e, must be determined from an inviscid analysis consistent with the imposed pressure distribution. The gas model adopted for the present study is thermally and calorically perfect air (or nitrogen) obeying the relations

$$\overline{p} = \overline{\rho} R \overline{T} \tag{9}$$

$$\overline{h} = c_p \overline{T} \tag{10}$$

with the specific heat ratio $\gamma = 1.40$, the gas constant R = 1,716 ft-lbf/slug-°R for air (1,776.29 for nitrogen), and the specific heat at constant pressure c_p = 6,006 ft-lbf/slug-°R for air (6,217 for nitrogen). The laminar viscosity is taken to obey Sutherland's law,

$$\overline{\mu} = 2.27 \times 10^{-8} \frac{\overline{T}^{3/2}}{\overline{T} + 198.6} \quad \frac{lbf-sec}{ft^2} \tag{11}$$

($\overline{T}$ is in degrees Rankine). The laminar Prandtl number, Pr, is assumed to have a constant value of 0.71 across the boundary layer; i.e.,

$$Pr = 0.71 \tag{12}$$

Following the development given in Appendix A of the report by Laster (Ref. 20), the continuity, energy, and streamwise momentum equations can be combined to yield the compressible time-averaged

11

turbulent kinetic energy equation for two-dimensional boundary-layer
flows. The approach of Laster in conjuction with equations equivalent
to Eqs. (1), (2), and (4) yields the compressible, time-averaged tur-
bulent kinetic energy equation valid for two-dimensional or axisymmetric
flows, which may be written in the form

$$1/r^j \; \partial/\partial x \left(1/2 \; r^j \; \bar{\rho} \; \bar{u} \; \overline{q^2} \right) + \partial/\partial y \left[1/2 \; (\bar{\rho} \; \bar{v} + \overline{\rho' \; v'}) \; \overline{q^2} \right]$$

$$= - (\bar{\rho} \; \overline{u' \; v'} + \overline{\rho' \; u' \; v'}) \; \partial \bar{u}/\partial y$$

$$+ \overline{p' \; \partial v'/\partial y} - \overline{\rho' \; u'} \; (\bar{u} \; \partial \bar{u}/\partial x + \bar{v} \; \partial \bar{u}/\partial y) - \bar{\rho} \; \overline{(u')^2} \; \partial \bar{u}/\partial x - \bar{\rho} \; \overline{(v')^2} \; \partial \bar{v}/\partial y$$

$$+ \partial/\partial y \left(1/2 \; \overline{\rho' \; v' \; q^2} \right) - \partial/\partial y \left(\overline{p' v'} + 1/2 \; \bar{\rho} \; \overline{v' \; q^2} + 1/2 \; \overline{\rho' \; q^2 \; v'} \right)$$

$$+ \partial/\partial y \left\{ \bar{\mu} \; \partial/\partial y \left[1/2 \; \overline{q^2} + \overline{(v')^2} \right] \right\} - \bar{\rho} \; \epsilon \tag{13}$$

where

$$\bar{\rho} \; \epsilon = \overline{\sigma'_{\ell m} \left(\frac{\partial u'_{\ell}}{\partial x_m} \right)} \tag{14}$$

represents the viscous dissipation of turbulent energy in conventional
tensor notation. Above, $1/2 \; \overline{q^2}$ denotes the turbulent kinetic energy, k,
defined as

$$k = 1/2 \; \overline{q^2} = 1/2 \left[\overline{(u')^2} + \overline{(v')^2} + \overline{(w')^2} \right] \tag{15}$$

A discussion of the physical meaning of each term in Eq. (13) is given
in section IV of chapter II in the report by Laster (Ref. 20) which also
contains a derivation of the compressible turbulent kinetic energy
equation in tensor notation. The paper by Bradshaw and Ferriss (Ref.
21) and the book by Cebeci and Smith (Ref. 8) contain similar deriva-
tions and discussions. Equation (13) has been derived using no assump-
tions or restrictions other than the classical boundary-layer order-of-

magnitude analysis used to eliminate certain terms from the complete turbulent kinetic energy equation. The turbulent kinetic energy equation [Eq. (13)] can be formally integrated from the wall (y = 0) to the edge of the boundary layer (y = δ) to obtain

$$\int_0^\delta \frac{1}{r^j} \partial/\partial x \left(1/2 \; r^j \; \overline{\rho} \; \overline{u} \; \overline{q^2}\right) dy + \left[1/2 \; (\overline{\rho} \; \overline{v} + \overline{\rho' v'}) \; \overline{q^2}\right]_0^\delta$$

$$= -\int_0^\delta \left(\overline{\rho} \; \overline{u'v'} + \overline{\rho' \; u' \; v'}\right) \partial\overline{u}/\partial y \; dy + \int_0^\delta \overline{p' \; \partial v'/\partial y} \; dy$$

$$- \int_0^\delta \left[\overline{\rho' u'} \; (\overline{u} \; \partial\overline{u}/\partial x + \overline{v} \; \partial\overline{u}/\partial y) + \overline{\rho} \overline{(u')^2} \; \partial\overline{u}/\partial x\right.$$

$$\left. + \overline{\rho} \; \overline{(v')^2} \; \partial\overline{v}/\partial y\right] \; dy + \left(1/2 \; \overline{\rho' \; v' \; q^2}\right)_0^\delta$$

$$- \left(\overline{p'v'} + 1/2 \; \overline{\rho} \; \overline{v' \; q^2} + 1/2 \; \overline{\rho' \; q^2 v'}\right)_0^\delta$$

$$+ \left\{\overline{\mu} \; \partial/\partial y \; \left[1/2 \; \overline{q^2} + \overline{(v')^2}\right]\right\}_0^\delta \; - \; \int_0^\delta \overline{\rho} \; \epsilon \; dy \tag{16}$$

Leibnitz's rule (Ref. 22) for differentiation of an integral depending upon a parameter must be used since the boundary-layer thickness, δ, is a function of the streamwise distance x; i.e., δ = δ(x). Thus the first integral in Eq. (16) can be written

$$\int_0^\delta \partial/\partial x \left(1/2 \; r^j \; \overline{\rho} \; \overline{u} \; \overline{q^2}\right) dy = d/dx \int_0^\delta r^j \; 1/2 \; \overline{\rho} \; \overline{u} \; \overline{q^2} \; dy$$

$$- 1/2 \; r^j \; \rho_e \; U_e \overline{q_e^2} \; d\delta/dx \tag{17}$$

where the subscript e denotes conditions at the edge of the boundary layer where y = δ. Since all turbulent quantities such as $\overline{q^2}$, $\overline{\rho'v'}$, etc., are identically zero at the wall (due to viscous damping) and since $\partial/\partial y \left[\frac{1}{2} \overline{q^2} + \overline{(v')^2}\right]$ is identically zero at both the wall and the boundary-layer edge, Eq. (16) may be written as

$$1/r^j \ d/dx \int_0^\delta r^j \ 1/2 \ \bar{\rho} \ \bar{u} \ \overline{q^2} dy = - \int_0^\delta (\bar{\rho} \ \overline{u'v'} + \overline{\rho'u'v'})$$

$$\partial \bar{u}/\partial y \ dy + \int_0^\delta \overline{p'\partial v'/\partial y} \ dy - \int_0^\delta \left\{ \overline{\rho'u'} \left[\bar{u} \ \partial \bar{u}/\partial x + \right. \right.$$

$$\left. \bar{v} \ \partial \bar{u}/\partial y \right] + \bar{\rho} \ \overline{(u')^2} \ \partial \bar{u}/\partial x + \bar{\rho} \ \overline{(v')^2} \ \partial \bar{v}/\partial y \right\} \ dy -$$

$$\int_0^\delta \bar{\rho} \ \epsilon \ dy + E \tag{18}$$

with the term E defined as

$$E = \left[1/2 \ \overline{q^2} \ (\bar{\rho} \ \bar{u} \ d\delta/dx - \bar{\rho} \bar{v}) - \overline{p'v'} - 1/2 \ \bar{\rho} \ \overline{v'q^2} \right.$$

$$\left. - 1/2 \ \overline{\rho' \ q^2 v'} \right]_e \tag{19}$$

The subscript e denotes that all quantities in the term E are to be evaluated at the edge of the boundary layer. Equation (18) is the IKET (integral kinetic-energy-of-turbulence) equation. A discussion of the physical meaning of the various terms in Eq. (19) will be given in Section 2.5.

2.2 TURBULENCE MODEL

The governing equations [Eqs. (1), (2), (4), and (18)] presented and examined in the preceding section do not in their present form con-stitute a complete system, since there are more dependent variables than equations. In particular, the fluctuating quantities introduced by the time-averaging process must be functionally related to the mean flow variables or additional partial differential equations provided for the fluctuating quantities; i.e., the problem of closure must be faced. Cebeci and Bradshaw (Ref. 23) discuss in an admirable manner the problem of closure and its ramifications. Turbulence models, plausible simpli-fying assumptions involving mathematical modeling of various turbulence quantities, are used to achieve closure and hence to reduce the number of dependent variables to the number of equations. It is via this modeling process (content and completeness) that this analysis differs markedly from the previous extended mixing-length investigations reported (Refs. 11-17).

The turbulent shear stress, τ_t, for compressible flow is given by

$$\tau_t = -\,\overline{\rho}\;\overline{u'v'} - \overline{\rho'u'v'} \tag{20}$$

Following the assumptions and approximations of Bradshaw and Ferriss (Ref. 21), namely that $\overline{\rho'u'v'} \ll \overline{\rho}\;\overline{u'v'}$, it is assumed that

$$\tau_t = -\,\overline{\rho}\;\overline{u'v'} \tag{21}$$

The Kolmogorov-Prandtl model of turbulence as presented by Wolfshtein (Ref. 24) is adopted so that

$$\tau_t = \mu_t\,\partial\overline{u}/\partial y \tag{22}$$

with the turbulent viscosity μ_t defined by

$$\mu_T = C_\mu\,\overline{\rho}\,k^{1/2}\,\ell_\mu \tag{23}$$

where C_μ is an empirical constant, k is the kinetic energy [defined by Eq. (15)] , and ℓ_μ is the length scale for turbulent shear stress. The dissipation, D, of turbulent energy is, following Wolfshtein (Ref. 24),

$$D = \overline{\rho}\,\varepsilon = \frac{C_D\,\overline{\rho}\,k^{3/2}}{\ell_D} \tag{24}$$

where C_D is an empirical constant and ℓ_D is the length scale for dissipation. In accord with Bradshaw, Ferriss, and Atwell (Ref. 18) and Townsend (Ref. 25),

$$-\,\overline{u'v'} = a_1\,\overline{q^2} = 2a_1\,k = \tau_t/\overline{\rho} \tag{25}$$

$$\overline{(u')^2} = a_2\,\overline{q^2} \tag{26}$$

$$\overline{(v')^2} = a_3\,\overline{q^2} \tag{27}$$

$$\overline{(w')^2} = (1 - \alpha_2 - \alpha_3)\,\overline{q^2} \tag{28}$$

The numerical values of a_1, a_2, and a_3 are generally ascribed constant values which are independent of the x- and y-coordinate directions. The work of Rose and Murphy (Ref. 26), however, established that a_1 is not a constant but is a function of the distance normal to the wall (the y-coordinate in this report); hence, $a_1 = a_1(y)$.

Terms involving the fluctuating density, ρ', are modeled following Bradshaw and Ferriss (Ref. 21) as

$$\rho'/\overline{\rho} \approx \overline{uu'}/\overline{h} \tag{29}$$

so that

$$\overline{\rho'u'} \approx (\overline{\rho u}/\overline{h}) \, \overline{(u')^2} = \frac{a_2 \overline{\rho u q^2}}{\overline{h}} = \frac{2a_2 \overline{\rho u k}}{\overline{h}} \tag{30}$$

and

$$\overline{\rho'v'} \approx \frac{\overline{\rho u \cdot u'v'}}{\overline{h}} = \frac{-\tau_t \overline{u}}{\overline{h}} \tag{31}$$

The fundamental assumptions leading to Eq. (29) are that (1) the fluctuation of total enthalphy is much less than the fluctuation of static enthalpy and (2) the pressure fluctuations are small if the Mach number fluctuation is much less than unity. It is also assumed that the term $(\gamma - 1)M^2$ is no greater than unity where M is the local time-averaged Mach number. Shamroth and McDonald (Ref. 13) discuss the relative importance of the pressure dilatation term, $\overline{p' \, \partial v'/\partial y}$, and conclude that it is small relative to the other terms in the turbulent kinetic energy equation. Combination of all the above assumptions essentially restricts the formal applicability of the resulting analysis to supersonic and low hypersonic flows with free-stream Mach numbers less than approximately five.

The turbulent heat flux, $\overline{\rho \ \widehat{v} \widehat{h}}$, is modeled via use of a turbulent Prandtl Number, Pr_t (based on the use of static enthalphy), by which the turbulent thermal conductivity is related to the turbulent viscosity as $Pr_t = c_p \ \mu_t / k_t$. The turbulent Prandtl number, Pr_t, is taken to be a constant value of 0.90 across the entire boundary layer.

The time-averaged quantities (such as $\overline{\widehat{u} \widehat{v}}$) appearing in the IKET equation [Eq. (18)] can now be related to the mean flow quantities and the various length and structural scales and constants introduced by the turbulence model. In particular, Eqs. (21), (22), (23), and (25) can be combined to yield

$$- \overline{\widehat{u} \ \widehat{v}} = \tau_t / \overline{\rho} = \left(\mu_t / \overline{\rho} \right) \partial \overline{u} / \partial y = C_\mu \ k^{1/2} \ell_\mu \ \partial \overline{u} / \partial y = 2a_1 k \qquad (32)$$

which results in

$$k^{1/2} = \left(C_\mu / 2a_1 \right) \ell_\mu \ \partial \overline{u} / \partial y \qquad (33)$$

so that the turbulent viscosity, μ_t, given by Eq. (23) becomes

$$\mu_t = \left(C_\mu^2 / 2a_1 \right) \overline{\rho} \ \ell_\mu^2 \ \partial \overline{u} / \partial y \qquad (34)$$

and hence the turbulent shear stress τ_t may be written as

$$\tau_t = \mu_t \ \partial \overline{u} / \partial y = \left(C_\mu^2 / 2a_1 \right) \overline{\rho} \ \ell_\mu^2 \ (\partial \overline{u} / \partial y)^2 \qquad (35)$$

The dissipation of turbulent energy, given by Eq. (24), can now be expressed as

$$D = \overline{\rho} \ \varepsilon = (C_D \overline{\rho} / \ell_D) \ \left[(C_\mu / 2a_1) \ \ell_\mu \ \partial \overline{u} / \partial y \ ^3 \right. \qquad (36)$$

Using the aforementioned relations, one can combine terms in Eq. (18), the IKET equation, to produce

$$1/r^j \ d/dx \int_0^\delta r^j \ \overline{\rho} \ \overline{u} \ \left(\ell_\mu/2a_1\right)^2 \ (\partial\overline{u}/\partial y)^2 \ dy$$

$$= \int_0^\delta \frac{\overline{\rho}\ell_\mu^2}{2a_1} \ (\partial\overline{u}/\partial y)^3 \left[1 - \frac{C_D \ C_\mu}{(2a_1)^2} \ (\ell_\mu/\ell_D)\right] dy$$

$$- \int_0^\delta \overline{\rho}(\ell_\mu/2a_1)^2 \ (\partial\overline{u}/\partial y)^2 \left[2a_2 \ (1 + \overline{u}^2/\overline{h}) \ \partial\overline{u}/\partial x\right.$$

$$\left. + \ 2a_2(\overline{u} \ \overline{v}/\overline{h}) \ \partial\overline{u}/\partial y + 2a_3 \ \partial\overline{v}/\partial y\right] dy + E/C_\mu^2 + E_r/C_\mu^2 \qquad (37)$$

The additional term involving E_r (reflecting wall roughness effects) will be explained in Section 2.4. A discussion of the physical meanings of the terms E and E_r will be given in Section 2.5.

2.3 LENGTH SCALES, STRUCTURAL SCALES, AND EMPIRICAL CONSTANTS

The implementation and effective use of Eq. (37) is dependent upon the length scales (ℓ_μ and ℓ_D), the structural scales (a_1, a_2, and a_3), and empirical constants (C_D and C_μ). A two-layer model of the turbulent boundary layer is adopted following the classical inner-outer region approach in which separate functional relationships are prescribed in each region with continuity of the functions between each region.

For the inner region, which includes the viscous sublayer, the length scales and the structural scale a_1 are taken as

$$\ell_\mu = y \ D_\mu \qquad (38)$$

$$\ell_D = y \ D_D \qquad (39)$$

$$a_1 = a_t \ D_a \qquad (40)$$

where D_μ, D_D, and D_a are damping functions which account for viscous sublayer effects and which are assumed, following Wolfshtein (Ref. 24), to be of the form

$$D_\mu = 1 - \exp(-A_\mu R_t) \tag{41}$$

$$D_D = 1 - \exp(-A_D R_t) \tag{42}$$

$$D_a = 1 - \exp(-A_a R_t) \tag{43}$$

with empirical constants A_μ, A_D, and A_a to be determined. In Eq. (40) the quantity a_t represents the fully turbulent value of the structural scale a_1, whereas R_t denotes a local turbulence Reynolds number defined as

$$R_t = \frac{\bar{\rho} \, k^{1/2} \, y}{\bar{\mu}} \tag{44}$$

The length scales and the structural scale a_1 for the outer region are of the form

$$\ell_\mu = Y \tag{45}$$

$$\ell_D = \lambda_D \delta \tag{46}$$

$$a_1 = a_t \tag{47}$$

where λ_D is an empirical constant, δ is the boundary-layer thickness, and Y is the outer region value of the length scale ℓ_μ. Continuity of the functional relationships is used to couple the inner- and outer-region values of ℓ_μ, ℓ_D, and a_1. That is, continuity is maintained between Eqs. (38) and (45), Eqs. (39) and (46), and Eqs. (40) and (47). The addition of the IKET equation allows one parameter normally taken as constant to be solved for in the streamwise (x) direction. Conventional mixing-length hypothesis turbulence models take ℓ_μ/δ to be a constant (usually 0.09 and written as λ/δ). The extended mixing-length hypothesis turbulence model examined in this report allows Y to be a variable

which is determined (i.e., calculated) by the IKET equation. The outer-region value of the length scale ℓ_μ, namely Y, is the one parameter to be determined from Eq. (37) and, hence, controls the streamwise development of the turbulent shear stress in such a way that the history of the turbulent state is considered explicitly.

The values of the nine empirical constants (C_μ, C_D, a_t, a_2, a_3, A_μ, A_D, A_a, and λ_D) introduced previously can be plausibly deduced using classical turbulent boundary-layer theory as well as recent experimental results involving compressible turbulent boundary-layer flows. Appendix A contains the details of such a process. The deduced values of the constants together with the values used by Wolfshtein (Ref. 24) are given in Table 1.

Table 1. Turbulence Model Empirical Constants

	Present Work	Wolfshtein[a]
C_μ	0.2383	0.220
C_D	0.3777	0.416
a_t	0.150	
a_2	0.566	
a_3	0.150	
A_μ	0.016	0.016
A_D	0.18885	0.263
A_a	0.0469	
λ_D	0.2069	

[a]Ref. 24

2.4 TURBULENCE MODEL MODIFICATIONS

The values of nine empirical constants contained in Table 1 represent a "baseline" turbulence model and should be viewed as valid for zero pressure gradient, no transpiration, and smooth-wall boundary-layer flows. Because of the intimate relationship which exists between the

surface condition (roughness, transpiration, etc), the pressure gradient, and the structure of the turbulent boundary layer near the surface, some of the constants listed in Table 1 can be expected to have magnitudes different from the baseline case.

As utilized in Appendix A the hypothesis of Morkovin (Ref. 27) (which states that the turbulent motion and structure in a compressible boundary layer should be equivalent to those of an incompressible boundary layer as long as the turbulent motion itself is incompressible -- usually implying a local Mach number less than five) permits the employment of the vast incompressible data on turbulent boundary-layer structure for turbulent compressible boundary layers. Thus the effects of roughness, transpiration, and pressure gradient which have been extensively and carefully ascertained from incompressible experiments can be used to infer changes in the nine constants of Table 1 from their baseline values.

These data suggest, at least within the context of the mixing-length concept, that the structure near the wall is most significantly affected. This corresponds in the inner-outer region analysis employed in this paper to the inner-region structure which is controlled by the constants A_D, A_a, and A_μ. The structural constants a_t, a_2, and a_3 are assumed to be essentially "universal" constants which are invariant over a wide range of conditions. The results of Rose and Murphy (Ref. 26) for a_t tend to confirm this, and by inference the Morkovin (Ref. 27) hypothesis supports this for a_2 and a_3. The constants C_D and C_μ apply across the entire boundary layer, both the inner and outer regions, and hence should vary only slightly and in particular should be independent of the values of the inner-region constants A_D, A_a, and A_μ. The remaining constant, λ_D, is germane only in the outer region and should not be directly coupled to the inner-region constants.

As demonstrated in Appendix A, the following equations may be deduced using the previously defined expressions for the present turbulence model and the existing data base for turbulent boundary-layer flows:

$$C_\mu = \kappa \sqrt{2a_t} \tag{48}$$

$$C_D = (2a_t)^{3/2} \Big/ \kappa \tag{49}$$

$$\lambda_D = \lambda/\kappa \tag{50}$$

$$A_D = 1/2 \frac{(2a_t)^2}{C_\mu} \tag{51}$$

$$A_a = \frac{A_{eff}^+}{2a_t \, \kappa} \, (A_\mu \, C_\mu)^{3/2} \tag{52}$$

$$A_\mu = 0.016 \tag{53}$$

Here κ is the von Kármán constant and A_{eff}^+ is the effective value of the constant in the classical van Driest (Ref. 28) damping expression. The term A_{eff}^+ may be interpreted as the effective thickness of the viscous sublayer expressed in terms of the inner-layer coordinates. It is well known (e.g., van Driest) that effects such as transpiration, pressure gradient, and roughness can be simulated by changing the damping expression since these effects tend to alter the sublayer thickness. Kays and Moffat (Ref. 29) and Healzer, Moffat, and Kays (Ref. 30) present empirical correlations of the above effects expressed in terms of A_{eff}^+, the classical van Driest damping parameter. An examination of Eqs. (51) through (53) indicates that A_a reflects a dependence upon A_{eff}^+ but that A_D and A_μ do not. Since the structure of the inner region must reflect the effects of transpiration, pressure gradient, and roughness, the expressions A_D and A_μ as given by Eqs. (51) and (53) must be altered. The forms chosen for A_D and A_μ will be given later in this report. At this point the realization that A_D and A_μ as well as A_a must be functions of A_{eff}^+ is sufficient.

In an inner- and outer-region model of the turbulent boundary layer the single most important parameter is the effective thickness of the viscous sublayer, A^+_{eff}. Although it constitutes only a small fraction of the boundary-layer thickness, the sublayer is the region wherein the major change in velocity occurs and where (except for low Prandtl number fluids) the most resistance to heat transfer takes place. Viewed in the context of the viscous sublayer, experimental evidence supports the concept that a favorable gradient ($d\bar{p}/dx$ negative) results in increased sublayer thickness, an adverse pressure gradient ($d\bar{p}/dx$ positive) results in decreased sublayer thickness, transpiration (blowing or suction) affects (decreases or increases) the sublayer thickness, and surface roughness results in decreased sublayer thickness.

Kays and Moffat (Ref. 29) recommend the following equations for the effective equilibrium value of the viscous sublayer thickness as a function of pressure gradient and wall transpiration velocity:

$$A^+_{eff} = \frac{26.0*}{a\left[v^+_w + b\left(\frac{p^+}{1 + c\,v^+_w}\right)\right] + 1} \tag{54}$$

where v^+_w is the wall transpiration velocity normalized by the friction velocity $u^+_w = \sqrt{\tau_w/\bar{\rho}_w}$ and p^+ is the dimensionless pressure gradient defined as $\left(\bar{v}_w/\bar{\rho}_w\,u^{+3}_w\right)d\bar{p}/dx$. The constants a and b are functions of p^+ and v^+_w and are

$$a = 7.1 \text{ for } v^+_w \geq 0 \quad \text{otherwise } a = 9.0$$
$$b = 4.25 \text{ for } p^+ \leq 0 \quad \text{otherwise } b = 2.0$$
$$c = 10.0 \text{ for } p^+ \leq 0 \quad \text{otherwise } c = 0.0$$

---

*24.0 as given by Ref. 29 but taken as 26.0 in this report for consistency with other empirical values.

The effects of pressure gradient and transpiration can be seen in Fig. 1, where Eq. (54) is parametrically plotted. Figure 1 graphically illustrates the high values which A_{eff}^+ assumes in the presence of strong favorable pressure gradients. These large values of A_{eff}^+ result in the viscous sublayer overwhelming the entire boundary layer (relaminarization) and in decreased heat transfer because of the increased resistence within the sublayer. Thus a considerable amount of physics is expressed by Eq. (54).
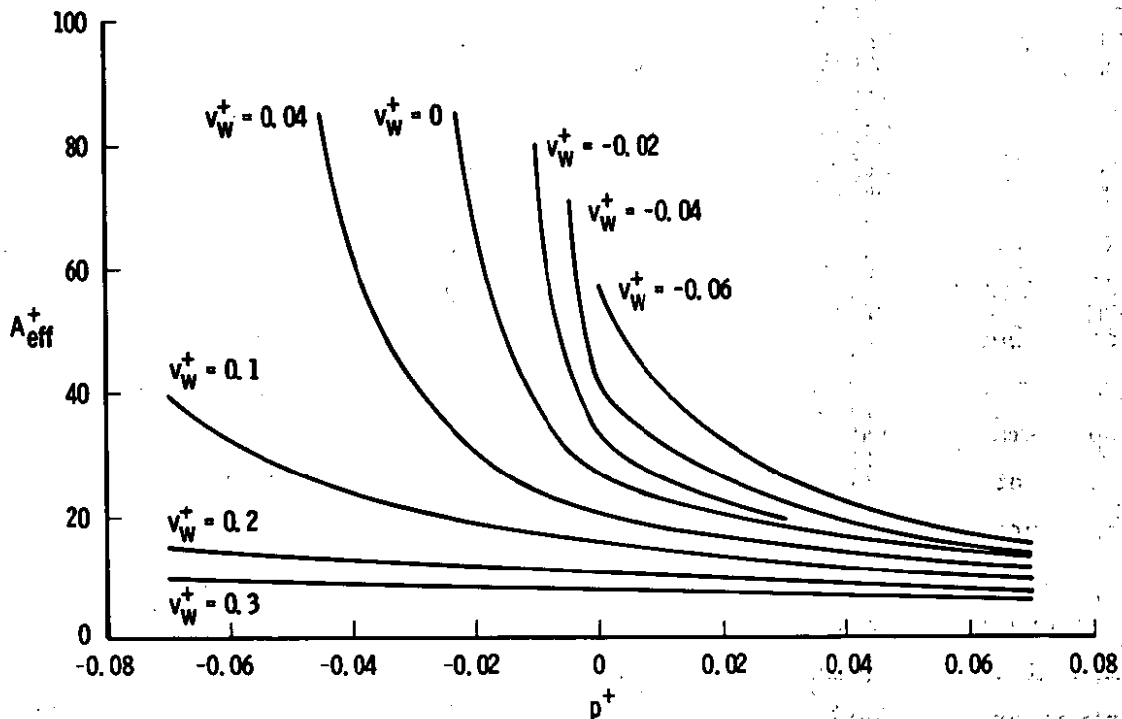
Figure 1. A_{eff}^+ as a function of pressure gradient and transpiration [Eq. (54)].

Equation (54) is essentially based upon the assumption of inner-region equilibrium and as such does not describe the manner in which A_{eff}^+ varies while changing from one equilibrium condition to another or while seeking an equilibrium condition. The recent paper of Horstman (Ref. 31) evaluates several approaches and concludes that a lag model in which A_{eff}^+ is a function of weighed upstream values of p^+ gives results superior to those of a rate model in which the rate of change of A_{eff}^+

is proportional to the difference between A^+_{eff} and the equilibrium value. In the lag formulation, $p^+(x)$ in Eq. (54) is replaced by $\overline{p^+(x)}$ where

$$\overline{p^+(x)} = \int_{x-2\lambda_\ell\delta}^{x} \omega(\zeta)\, p^+(\zeta)\, d\zeta \tag{55}$$

and

$$\omega(\zeta) = \frac{1}{\sqrt{2\pi}\,\sigma} \exp\left[-\,|\zeta - (x - \lambda_\ell\delta)|^2/2\sigma^2\right] \tag{56}$$

with

$$\sigma = \frac{\lambda_\ell\delta}{3} \tag{57}$$

where λ_ℓ is the lag length parameter. The basic effect of the lag formulation is not to diminish or enhance the effect of pressure gradient but to shift the effect downstream. Horstman makes no attempt to prescribe λ_ℓ as a function of x, but he does suggest that λ_ℓ should be much smaller for favorable pressure gradients than for adverse pressure gradients. Values of 20 and 10 were used for adverse and favorable pressure gradients, respectively. These values of λ_ℓ do not represent the optimum physics for every flow condition, but they do represent reasonable values. Horstman (Ref. 31) states that additional experimental data are needed for values of p^+ between 0.01 and 0.06 for a wide range of Reynolds numbers in order to develop a realistic correlation.

The results of Glowacki and Chi (Ref. 32), as presented by Horstman, indicate that the von Kármán constant, κ, is not a universal constant but is mildly dependent upon the pressure gradient. In particular they suggest that

$$\kappa = 0.435 + 0.182257\left[1 - \exp(-0.32068\beta)\right] \tag{58}$$

where β is a dimensionless pressure gradient defined as $\delta_i^* (d\bar{p}/dx)/\tau_w$ with δ_i^* as the kinematic displacement thickness. As with A_{eff}^+ in Eq. (54) this represents an equilibrium value of κ. The lag analysis can be applied to κ by replacing β in Eq. (58) with $\bar{\beta}$ where

$$\bar{\beta}(x) = \int_{x-2\lambda_\ell \delta}^{x} \omega(\zeta) \ \beta(\zeta) \ d\zeta \qquad (59)$$

with $\omega(\zeta)$ defined in Eq. (56). Glowacki and Chi recommend that Eq. (58) be used for flows with the dimensionless pressure gradient $\beta > 0$ and imply that the equation can be used for $\beta < 0$. In this report for $\beta \leq 0$ ($d\bar{p}/dx \leq 0.0$) the von Kármán constant κ was taken to be defined by Eq. (59) with the stipulation that κ must be greater than 0.05.

The value of A_{eff}^+ (and perhaps κ) calculated in the above manner must now be related to the inner-region empirical constants as given in Eqs. (48) through (53).

Equations (48) through (50) and Eq. (52) reflect, in a logical manner, the importance of κ and A_{eff}^+ on the constants C_μ, C_D, λ_D, and A_a and are used in this analysis. However, as previously mentioned, Eqs. (51) and (53) for A_D and A_μ do not adequately reflect changes in the inner region because of transpiration, pressure gradient, and roughness. Hence, changes in A_{eff}^+ (as predicted by the lag approach, for example) alter the length scale for mixing and must be reflected in the formulation used. Because of differences in the behavior of Eq. (38) and the classical van Driest relationship as the wall is approached, no unambiguous relationship is evident, but inspection of the two models suggests that A_μ and A_{eff}^+ should be related in an inverse manner. The relationship used in this analysis is

$$A_\mu = \frac{10.816}{\left(A_{eff}^+\right)^2} \qquad (60)$$

which reduces to $A_\mu = 0.016$ for $A^+_{eff} = 26.0$. Equation (60) has been adequate for a wide range of values of A^+_{eff}. In a similar vein, A_D, the damping constant for the dissipation length scale, has been taken as

$$A_D = 1/2 \frac{(2a_t)^2}{C_\mu} \sqrt{\frac{A_\mu}{0.016}} \tag{61}$$

These equations were verified by computer experimentation and were used unaltered for a wide variety of conditions examined in Section 3.0 of this report.

The modifications made to the baseline turbulence model to account for the effects of surface roughness are more extensive than, although similar to, those required for pressure gradient effects. The roughness model formulated uses the approach of Healzer, Moffat, and Kays (Ref. 30) in conjunction with the analysis of Finson (Ref. 33). The usual method of examining and presenting boundary-layer data over rough surfaces is to classify the surface as smooth, transitional, or fully rough according to the local value of the roughness Reynolds number

$$R_\tau = \frac{u^+_w k_r}{\bar{\nu}_w} \tag{62}$$

where u^+_w is the wall friction velocity. The surface is considered smooth aerodynamically if R_τ is less than 5.0 and the surface is fully rough for R_τ greater than 55.0 (although Schlichting (Ref. 34), for example, suggests 70.0); otherwise, the surface is transitionally rough. For boundary-layer flows with R_τ less than 5.0 the surface is taken as smooth with no resulting effects of roughness.

The model for the transitional roughness regime will now be developed. Following Healzer et at. (Ref. 30), the effect of roughness in this regime can be viewed as reducing the sublayer thickness which, in

27

turn, can effectively be controlled by decreasing A_{eff}^+ and hence [through Eq. (60)] increasing A_μ. The functional relationship is taken as

$$A_{eff}^+ = A^+ \frac{4.007 - \ell n \, R_\tau}{f} \qquad (63)$$

where

$$f = 1.299 \text{ ("uniform" roughness)}$$
$$2.061 \text{ (sand grain roughness)}$$
$$3.196 \text{ (commercial roughness)}$$

and A^+ in Eq. (63) is taken as A_{eff}^+ from Eq. (54). Equation (60) is then used to relate A_{eff}^+ to A_μ. The quantity f in Eq. (63) is a function of the uniformity of the roughness. The value of f varies from 3.196 for commercial roughness, which is completely random in shape and size distribution, to 1.299 for uniform shape, size, and packing distribution. Physically, this corresponds to a more rapid thinning of the sublayer by the more random roughness. Figure 2 illustrates Eq. (63) for each of the three values of f as a function of R_τ with A^+ taken as 26.0. The quantity $(4.007 - \ell n \, R_\tau)/f$ cannot exceed 1.00 in value as this would correspond to a thickening of the viscous sublayer by roughness, which is contrary to physical reality.

The regime of fully rough turbulent flow ($R_\tau > 55.0$) is predicted using the approach of Finson (Ref. 33). Physically, this regime corresponds to the situation in which the viscous sublayer has been destroyed. Thus A_{eff}^+ is effectively zero and the inner region damping terms D_μ, D_D, and D_a [as given in Eqs. (41) through (43)] tend toward 1.0. In Finson's model, which is postulated to be valid for three-dimensional roughness elements less than the boundary-layer thickness, the individual elements are considered, assuming attached parallel flow approaching the elements. The roughness elements each provide a distributed drag for the mean momentum equation, and each wake provides a source for the generation and dissipation of turbulent kinetic energy.

Each element (and all elements are identical in this model) has a diameter $D_r(y)$ which is a function of the distance from the wall and an average center-to-center spacing ℓ_r.
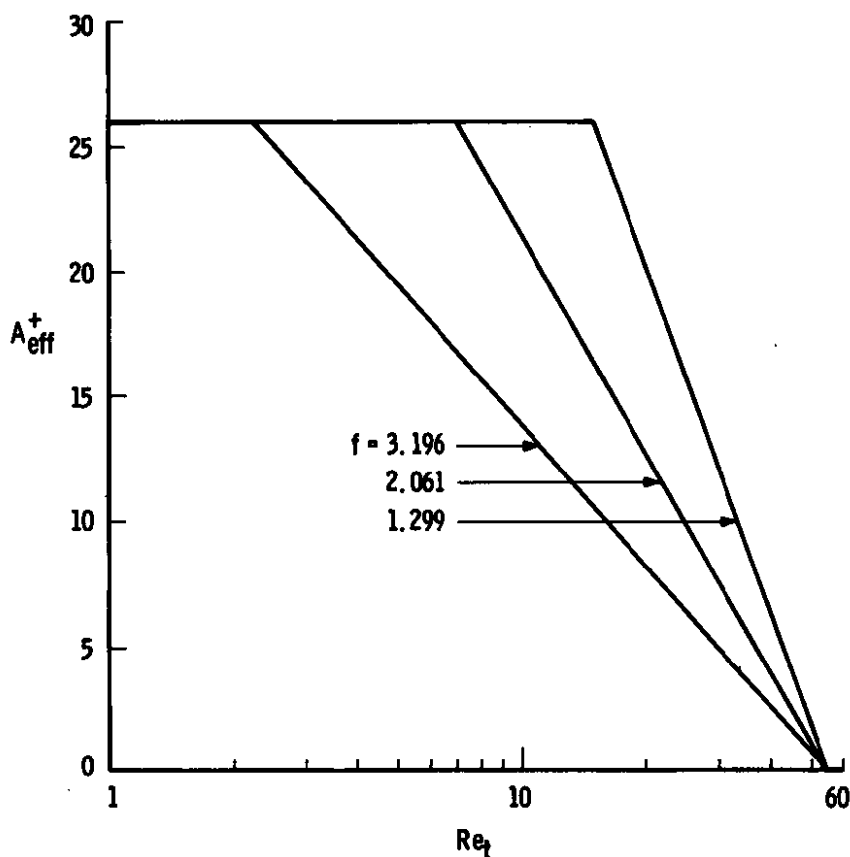
Figure 2. A_{eff}^+ as a function of f for the transitional roughness regime.

The form drag on roughness elements represents a sink term for the streamwise momentum equation. Referring to the following sketch, the drag between $(y - \delta y/2)$ and $(y + \delta y/2)$ on a single element is

$$-\tfrac{1}{2}\, \bar{\rho}\, \bar{u}^2 C_{D_r}\, D_r(y)\, \delta y \qquad (64)$$
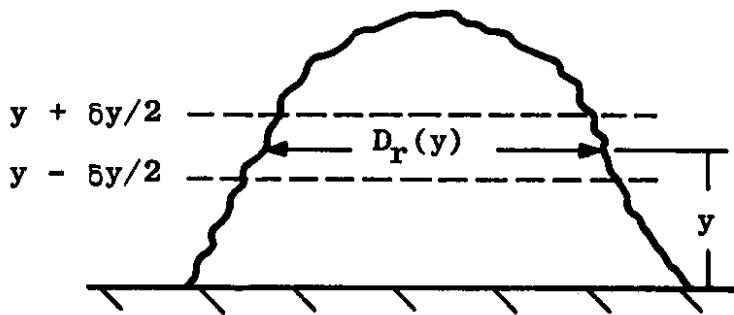
There are ℓ_r^{-2} roughness elements per unit surface area so that the momentum sink per unit differential volume is

$$-1/2 \; \overline{\rho} \; \overline{u}^2 \; c_{D_r} \; \frac{D_r(y)}{\ell_r^2} \tag{65}$$

where the recommended value of c_{D_r} is 0.5 with a roughness element spacing of ℓ_r. Finson (Ref. 33) suggests that for sand grain roughness, hemispherical elements spaced about two base diameters apart yield meaningful results. Equation (65) represents the additional term which appears in Eq. (2), the streamwise momentum equation, and is utilized only when fully rough turbulent flow is being calculated. The velocity fluctuations behind an element are taken as

$$u' \sim Q_u \; \overline{u} \tag{66}$$

where Q_u is of $\mathcal{O}(0.1)$. The turbulent kinetic energy generation per unit differential volume is

$$Q_u^2 \; \overline{\rho} \; \overline{u}^3 \; \frac{D_r(y)}{\ell_r^2} \tag{67}$$

For use in the IKET equation, this term is integrated over roughness height, k_r, resulting in

$$E_r = \int_0^{k_r} Q_u^2 \; \overline{\rho} \; \overline{u}^3 \; \frac{D_r}{\ell_r^2} \; dy \tag{68}$$

30

The term E_r is then added to Eq. (37) and represents the turbulent kinetic energy generation which occurs because of the wakes of the roughness elements. A dissipation term could also be included, but Finson found that this had little effect. Section 2.5 contains a discussion of the interpretation and importance of the term E_r, which appears in the IKET equation. The skin friction, or more properly, the flow resistance is taken as the sum of the integrated form drag of the elements and the pure frictional force applied to the whole surface; i.e.,

$$C_{f_\infty} = \frac{2 \, \overline{\mu}_w}{\rho_\infty u_\infty^2} \left[\frac{\partial \overline{u}}{\partial y} \right]_w + \int_0^{k_r} \frac{\overline{\rho} \, \overline{u}^2}{\rho_\infty u_\infty^2} C_{D_r} \frac{D_r}{\ell_r^2} \, dy \qquad (69)$$

Furuya, Miyata, and Fujita (Ref. 35) express the data from their experimental study of rough wall flows in such a manner.

All of the roughness examined in this paper was assumed to be of the sand grain type. This is obviously an optimistic assumption which greatly facilitates analysis but does not conform to the roughness element geometry expected in aerodynamics. For other than sand grain roughness the results of Dirling (Ref. 36), shown in Fig. 3, are used to relate various roughness geometries to an effective sand grain size, and that effective sand grain size is used in the rough-wall analysis. Reda, Ketter, and Fan (Ref. 37) point out situations in which the Dirling correlation should be used with caution.

2.5 IKET EXTERNAL SOURCE TERMS

The IKET equation as given by Eq. (37) contains the quantities E and E_r, which represent sources of turbulent kinetic energy in terms of a global energy balance. The IKET equation in effect assimilates the source terms E and E_r by varying the value of the outer region length scale ℓ_μ, namely Y. Local values of quantities such as the turbulent

2-D Rod Elements

- ■ Bettermann
- ◆ Liu et al.
- ◆ Streeter

3-D Elements - Schlichting

- ○ Spheres
- ◖ Spherical Segments
- △ Cones
- □ Cubes - Koloseus

2-D Wavy Surface

- ● Streeter
- ◕ Haughton

3-D Liquid Patterns

- △ Cohen

Recommended Correlation Curve

$$k_e/k_a = 0.0164 \ \Lambda^{3.78}$$

For $\Lambda \leq 4.93$

$$= 139 \ \Lambda^{-1.90}$$

For $\Lambda > 4.93$

From Ref. 36

$$\Lambda = \frac{\ell_r}{k_a}\left(\frac{A_s}{A_p}\right)^{4/3}$$
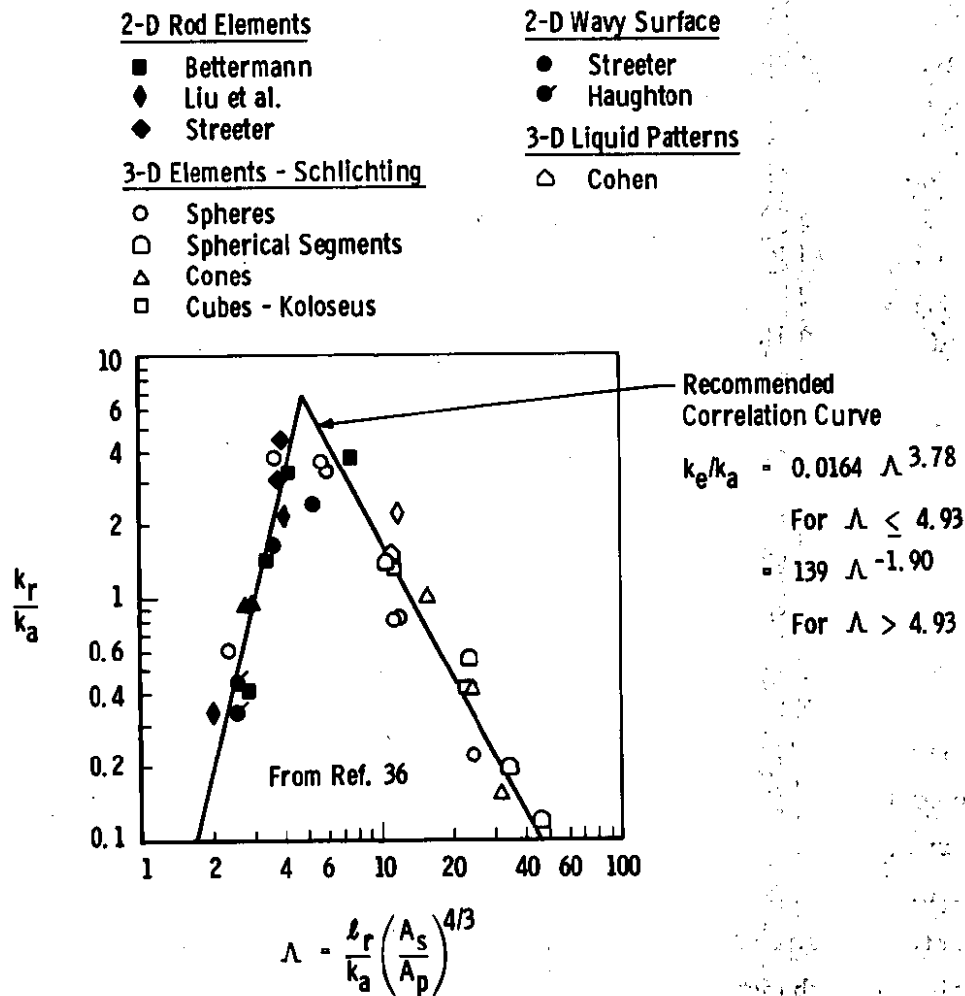
Figure 3. Effective sandgrain roughness correlation.

kinetic energy and the turbulent shear stress are then determined by the turbulence model using the distributions of the length scales ℓ_μ and ℓ_D and the structural scale a_1.

Physically, the various terms which comprise the quantity E defined by Eq. (19) represent turbulence source terms resulting from disturbances imposed upon the boundary layer by the free stream. The quantity E is actually the sum of two contributions, the first,

$$\left[1/2 \ \overline{q^2} \ (\overline{\rho} \ \overline{u} \ d\delta/dx \ - \ \overline{\rho} \ \overline{v})\right]_e \tag{70}$$

representing the <u>free-stream</u> turbulence entrained by the boundary
layer, and the second,

$$\left(-\overline{p'v'} \ - \ 1/2 \ \overline{\rho} \ \overline{v'q^2} \ - \ 1/2 \ \overline{\rho' \ q^2 \ v'}\right)_e \tag{71}$$

representing the direct absorption of <u>free-stream</u> acoustic energy by the
boundary layer. Both constituents of E then refer to quantities at the
outer edge of the boundary layer.

The quantity E_r, defined by Eq. (68), represents the turbulent
kinetic energy generation related to the wakes of individual roughness
elements and has much the same effect on the IKET equation as E does.
But unlike E, which is characterized by values at the edge of the
boundary layer, E_r depicts the turbulent kinetic energy generation (by
the roughness element wakes) <u>integrated</u> across the roughness element
geometry. The form of Eq. (68) is clearly indicative of the integrated
nature of E_r as well as of the dependence upon local conditions and the
geometric shape. Simply stated, free-stream turbulence, free-stream
acoustic disturbances, and/or roughness element wake turbulence serve to
provide a small source term for the IKET equation.

It is this source which mathematically "triggers" the transition
process from laminar to turbulent flow. McDonald and Fish (Ref. 12) and
Shamroth and McDonald (Ref. 13) present good discussions concerning
initiation of transition based on the IKET formulation. However, Eq.
(25) for the turbulent shear stress is strictly applicable only under
conditions of negligible or small levels of free-stream turbulence.

Hence, the present IKET formulation is restricted to negligible or small free-stream turbulence levels. A recent paper by McDonald and Kreskovsky (Ref. 14) shows how this restriction may be removed.

The capability to assimilate additional energies can hardly be overemphasized as it allows the transition process to be computed in a continuous fashion from completely laminar to fully developed turbulent flow. Within the constraints of the current analysis, transition can be triggered by absorption of incident acoustic energy and/or roughness-element-generated turbulent kinetic energy. These points will be examined further in Section 3.0.

2.6 NUMERICAL SOLUTION OF THE COMPRESSIBLE TURBULENT BOUNDARY-LAYER EQUATIONS

The governing compressible time-averaged boundary-layer equations, either two-dimensional or axisymmetric, as given by Eqs. (1) through (4), as well as the IKET equation defined by Eq. (37), are transformed to Illingworth-Levy variables and formulated into linearized finite-difference equivalents; the finite-difference forms are solved using an iterative, marching, implicit integration technique using tridiagonal matrices. Full details of the numerical approach may be found in Appendixes III and IV of the reports by Adams (Refs. 38 and 39). The digital computer code is written in FORTRAN IV with double-precision arithmetic for execution on an IBM 370/165; core storage is 180K bytes using the FORTRAN H OPT = 2 compiler. As with other parabolic boundary-layer codes, outer-edge conditions must be specified from a separate source, an inviscid analysis or an experimental pressure distribution, for example. The code features two-dimensional or axisymmetric flow, sharp or blunt leading edges (or noses), variable grid spacing in both streamwise and normal directions, and arbitrary wall temperature distribution (or adiabatic wall).

It should be noted that in the inner region ℓ_μ and a_1 form a coupled nonlinear set of algebraic equations at a given y-location, namely

$$\ell_\mu = y \left[1 - \exp\left(- \frac{A_\mu C_\mu}{2a_1} \frac{\overline{\rho}\ell_\mu y}{\overline{\mu}} \frac{\partial\overline{u}}{\partial y} \right) \right] \qquad (72)$$

and

$$a_1 = a_t \left[1 - \exp\left(- \frac{A_a C_\mu}{2a_1} \frac{\overline{\rho}\ell_\mu y}{\overline{\mu}} \frac{\partial\overline{u}}{\partial y} \right) \right] \qquad (73)$$

Newton's method as described by Conte and de Boor (Ref. 40) is used to solve the coupled system. The outer-region length scale $\ell_\mu = Y$ appears as a quadratic function in the IKET equation whose solution is numerically determined using Newton's method for root extraction as given by Householder (Ref. 41). A global iteration procedure is necessary in solving for the outer-region length scale Y because this value is linked with the inner-region scales through the requirements of functional continuity.

3.0 RESULTS AND DISCUSSION

3.1 INCOMPRESSIBLE FLAT PLATE FLOW

One of the classical experimental investigations often used for comparison with analytical theories is that of Klebanoff (Ref. 42), performed some 20 years ago in the National Bureau of Standards 4-1/2-ft low-speed wind tunnel. An artificially thickened, turbulent boundary layer was allowed to develop on a smooth flat plate 12 ft long. The scheme of artificially thickening the turbulent boundary layer was achieved by covering the first two feet of the plate with No. 16 floor-sanding paper. Boundary-layer probe surveys were made 10.5 ft from the leading edge, at which point the boundary-layer thickness was about 3 in. At this location the virtual origin, assuming a smooth surface, was

14.2 ft. The corresponding length Reynolds number based on values of x measured from the <u>virtual</u> origin was 4.2×10^6 with a free-stream velocity of 50 ft/sec.

Presented in Fig. 4 is a comparison of the mean velocity distribution as measured by Klebanoff, and the IKET-computed mean velocity distribution. The agreement is excellent. Also illustrated in Fig. 4 are the locations of the inner and outer regions, as well as the near-wall region. The computed turbulent shear stress distribution presented in Fig. 5 agrees as well with Klebanoff's data as did the mean profile. The IKET wall shear stress value (denoted by *) is in good agreement with the classical Squire-Young (Ref. 43) correlation. The near-wall region where the turbulent shear stress is damped to zero is not shown in Fig. 5.

Figure 6 presents a comparison between the IKET-computed turbulent kinetic energy distribution, the measured turbulent kinetic energy
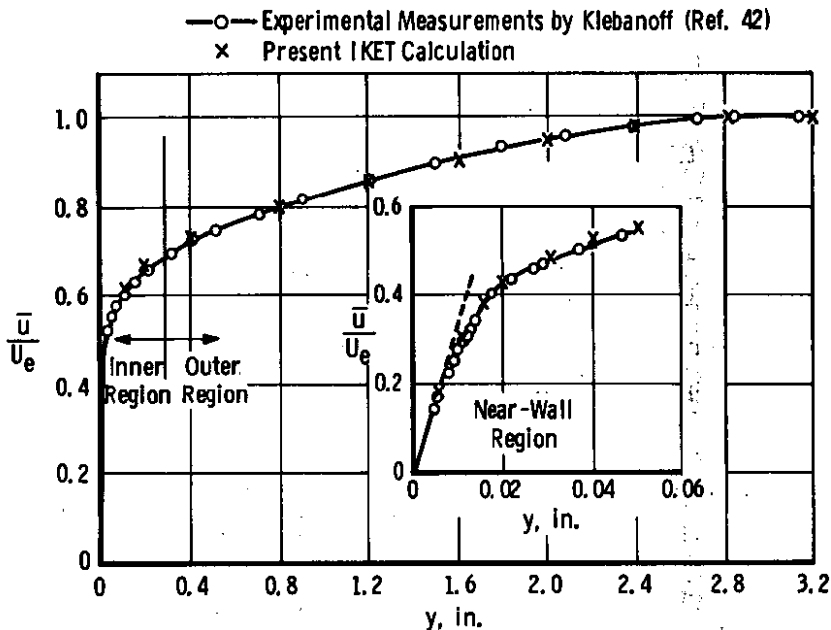
Figure 4. Mean-velocity distribution for fully developed incompressible turbulent boundary layer.

—o— Experimental Measurements by Klebanoff (Ref. 42)
×   Present IKET Calculation
∗   Wall Shear Stress from Present IKET Calculation
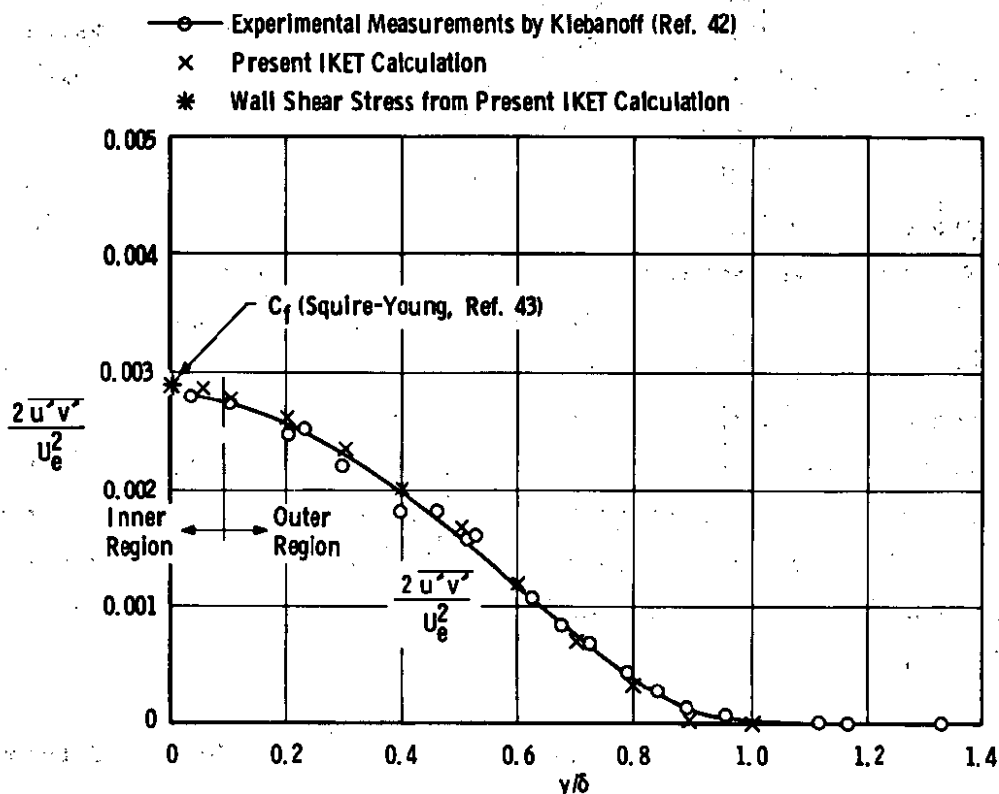
Figure 5. Distribution of turbulent shearing stress.

distribution, and a turbulent kinetic energy distribution computed by
Finson et al. (Ref. 44) using a multi-equation turbulence model. In the
outer region the IKET calculation is in good agreement with the data,
but in the inner region and the near-wall region the experimental
measurements are different in both character and numerical value from
the IKET calculation and the more sophisticated approach of Finson et
al. The experimental measurements of Klebanoff as presented in Fig. 6
exhibit a very small amount of free-stream turbulence which is reflected
in the constant turbulent kinetic energy distribution for values of y
greater than the boundary-layer thickness. The IKET analysis as exam-
ined in this report assumes zero free-stream turbulence at the edge of
the boundary layer. The paper by McDonald and Kreskovsky (Ref. 14)
shows how the restriction of zero free-stream turbulence may be removed.
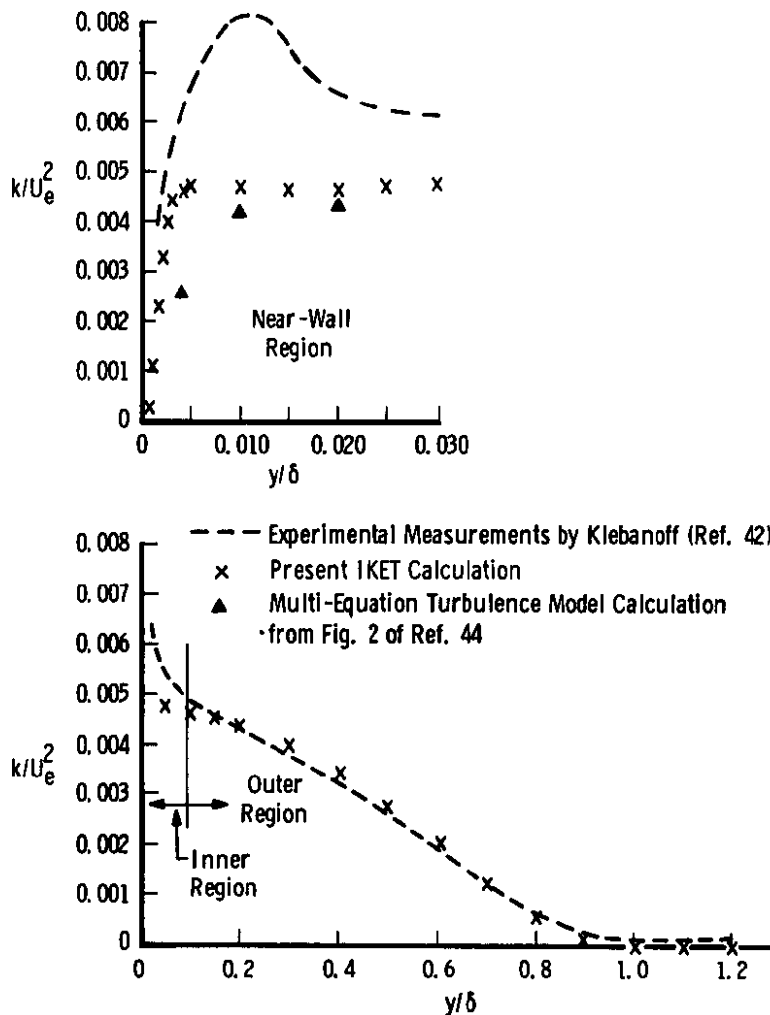
Figure 6. Distribution of turbulent kinetic energy in fully
developed incompressible turbulent boundary layer.

3.2 COMPRESSIBLE TURBULENT BOUNDARY-LAYER RELAMINARIZATION

The prediction of relaminarization phenomena is one of the most stringent tests of the innate "physics" of turbulence models. Relaminarization is basically a reversion from turbulent to laminar boundary-layer flow caused by sustained flow acceleration effects such as occur

in the subsonic contraction section of a nozzle. One of the best documented experimental investigations of compressible relaminarization is that reported by Nash-Webber (Ref. 45). In this work an instrumented flat plate was opposed by a variety of upper-wall profiles; the profiles were chosen to impose various pressure gradients on the flat-plate turbulent boundary layer. Figure 7 illustrates the edge velocity and
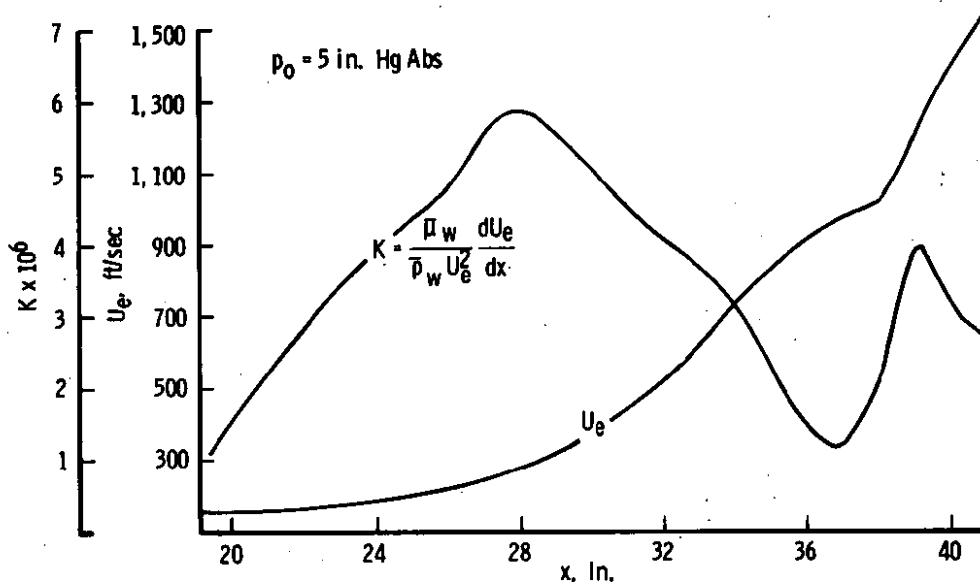
Figure 7. Velocity and acceleration parameter distribution for Nash-Webber Nozzle A.

the free-stream acceleration parameter K for the particular upper wall (Nozzle A) used in the IKET calculation. The free-stream acceleration parameter is defined as

$$K = \frac{\overline{\mu}_w}{\overline{\rho}_w \, U_e^2} \frac{dU_e}{dx} \tag{74}$$

where the w subscript denotes wall conditions and the e subscript denotes boundary-layer edge conditions. The importance of this parameter is illustrated by Fig. 8, taken from Ref. 45, which shows that the

39
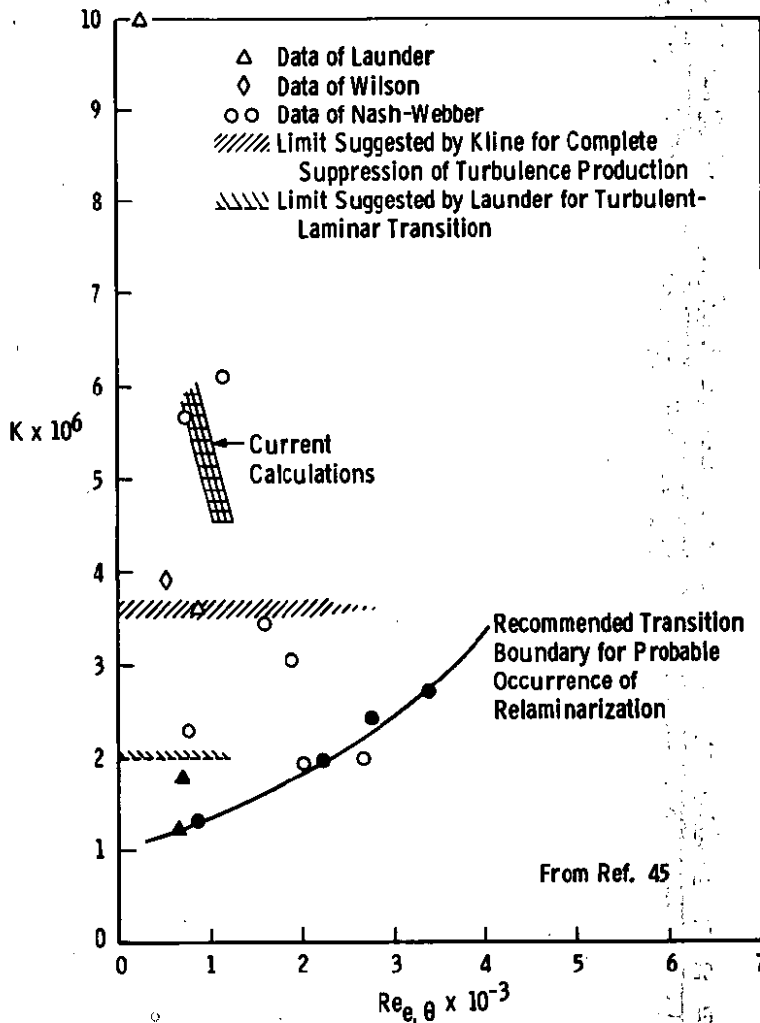
Figure 8. Turbulent-laminar transition boundary for adiabatic wall shear layer.

numerical value of K can be used as an indicator for the probable occurrence of relaminarization provided the momentum thickness Reynolds number based on edge conditions is sufficiently low. Presented in Fig. 9 are calculated results from the present IKET analysis and the experimental data of Nash-Webber. Calculated fully laminar and fully turbulent results are also shown for comparison purposes. The present IKET results are in good agreement with the experimental data. The local momentum thickness Reynolds number does not attain a laminar value until $x \approx 35$ in., which is well after the local skin friction attains its

laminar value ($x \approx 31$ in.). This is due to profile relaxation effects of the boundary-layer <u>upstream</u> <u>history</u>, a feature not possessed by conventional mixing-length analyses. Kreskovsky, Shamroth, and McDonald (Ref. 46) used a similar IKET analysis in their parametric study of relaminarization. They also examined the Nash-Webber Nozzle A flow and reported good agreement between their IKET analysis and experimental measurements.
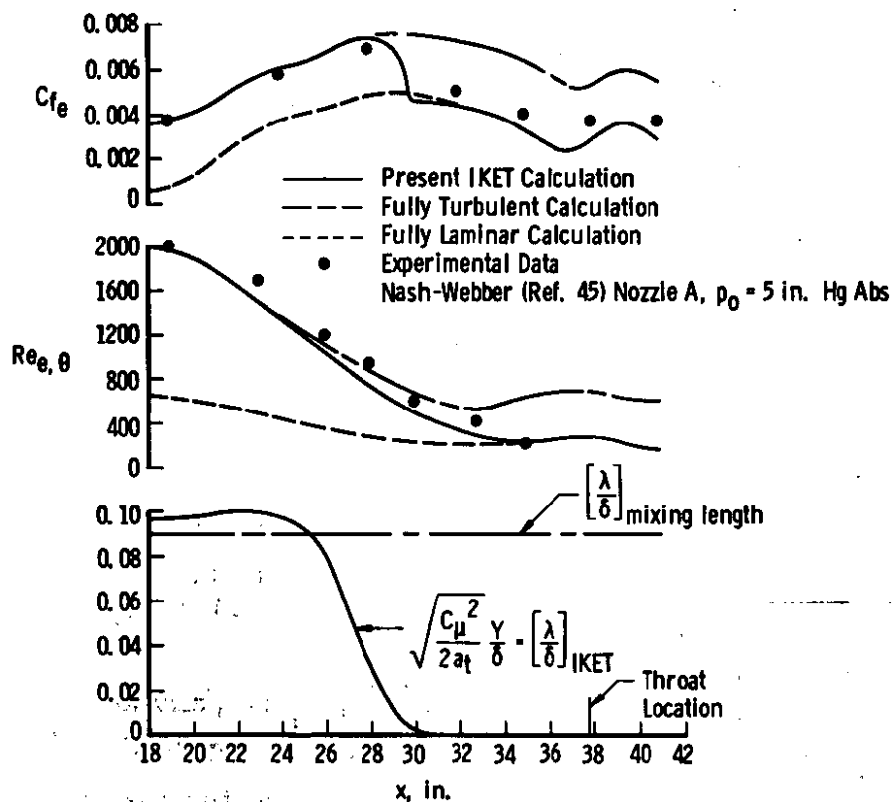
Figure 9. IKET calculation of turbulent boundary-layer relaminarization.

In Fig. 9 the equation

$$\sqrt{\frac{C_\mu^2}{2a_t}} \quad \frac{Y}{\delta} = \left[\frac{\lambda}{\delta}\right]_{IKET} \tag{75}$$

41

simply indicates the IKET extended mixing-length expression, which is equivalent to the conventional mixing-length ratio of the outer-region mixing length to the boundary-layer thickness. Conventional mixing-length analyses nominally assign 0.09 to this ratio, but the IKET extended mixing-length approach computes the ratio in the streamwise direction. The value of $[\lambda/\delta]_{IKET}$ is initially characteristic of turbulent flow, but as the large values of K are approached ($x \approx 28$ in.) the turbulent boundary layer begins to undergo relaminarization, which is reflected in the decreasing value of $[\lambda/\delta]_{IKET}$. At the x-location where the skin friction approaches the laminar value, the IKET computed value of $[\lambda/\delta]_{IKET}$ approaches zero, effectively resulting in laminar flow. Figure 9 also points out that the value of $[\lambda/\delta]_{IKET}$ starts to decrease, indicating the beginning of relaminarization, well before any effect on the skin friction is felt. This indicates that the outer-region length scales are being altered by the pressure gradient well before any effects are felt by the wall. Thus the IKET analysis possesses something akin to the "precursor" effect (See Section 3.4) in relaminarizing turbulent boundary-layer flows. Figure 9 also shows that the local momentum thickness Reynolds number based upon boundary-layer edge conditions is low (about 2,000 at the $x = 18$-in. location); therefore, according to Fig. 8, the upstream turbulent boundary layer is indeed a candidate for relaminarization, provided that the acceleration parameter K is of sufficient magnitude. By comparing the results of Fig. 9 with the acceleration parameter K given in Fig. 8, one can see that relaminarization occurred over the region where the numerical value of K was greater than 4×10^6. The crosshatched region in Fig. 8 corresponds to the current numerical example of the Nash-Webber Nozzle A and confirms the basic limits of validity for relaminarization as given by Kline and Launder in Fig. 8. An additional example of relaminarization-like behavior, a rough hemisphere-cylinder, will be examined in Section 3.7.

3.3 COMPRESSIBLE TURBULENT BOUNDARY LAYERS IN ADVERSE AND FAVORABLE PRESSURE GRADIENTS

One of the best experimental studies concerning compressible turbulent boundary-layer flows under nonequilibrium conditions is that reported by Lewis, Gran, and Kubota (Ref. 47) and Gran, Lewis, and Kubota (Ref. 48). Details of the AEDC von Kármán Gas Dynamics Facility (VKF) Supersonic Wind Tunnel (A) experiment may be found in the report of Hahn and Lutz (Ref. 49). The wind tunnel model, shown in Fig. 10, consisted of two parts: an outer, hollow shell whose walls can be cooled, and an
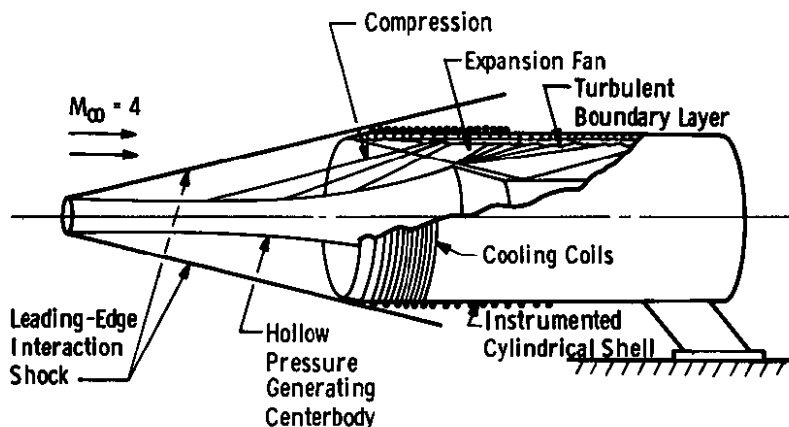
Figure 10. Gran, Lewis, and Kubota wind tunnel model schematic.

inner, pressure-generating body. The inner, pressure-generating body was contoured so that both compression and expansion regions were imposed on the outer shell. All boundary-layer measurements (temperature, pressure, heat flux, and profile surveys) were performed on the inner surface of the outer shell. Nominal free-stream conditions were

$$M_\infty = 3.98$$
$$Re_\infty/in. = 5.18 \times 10^5$$
$$T_{0,\infty} = 573°R$$

43

with model wall temperature ratios of

$$T_w/T_{o,\infty} = 0.9175 \text{ (hot wall)}$$
$$T_w/T_{o,\infty} = 0.50 \text{ (cold wall)}$$

As shown in Fig. 11, the centerbody was such that a zero pressure gradient initially existed (first 13.5 in. of the model); this was followed by an adverse pressure gradient (from 13.5 to 18.5 in of the model), and finally by a favorable pressure gradient (over the remainder of the model). The severe adverse pressure gradient increased the surface pressure by a factor of approximately 9 in a streamwise distance of only 5 in. Figure 11 also illustrates the Mach number variation along the model (analytical expressions are given in Refs. 47 and 48).
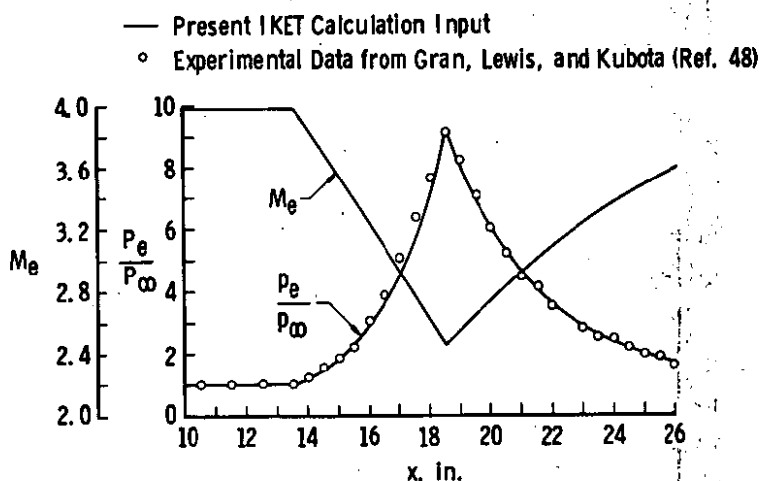
Figure 11. Edge Mach number and pressure distribution of inner wall of Gran, Lewis, and Kubota model.

Comparison of the IKET calculations and the experimental data are presented in Figs. 12 through 15 with respect to displacement thickness, momentum thickness, skin friction, and Stanton number distributions,
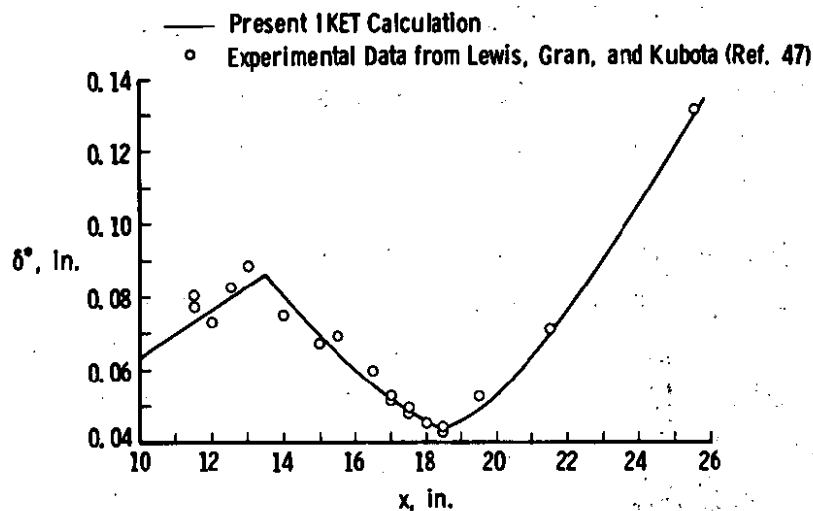
Figure 12. Displacement thickness distribution for hot-wall
condition for Gran, Lewis, and Kubota edge conditions.
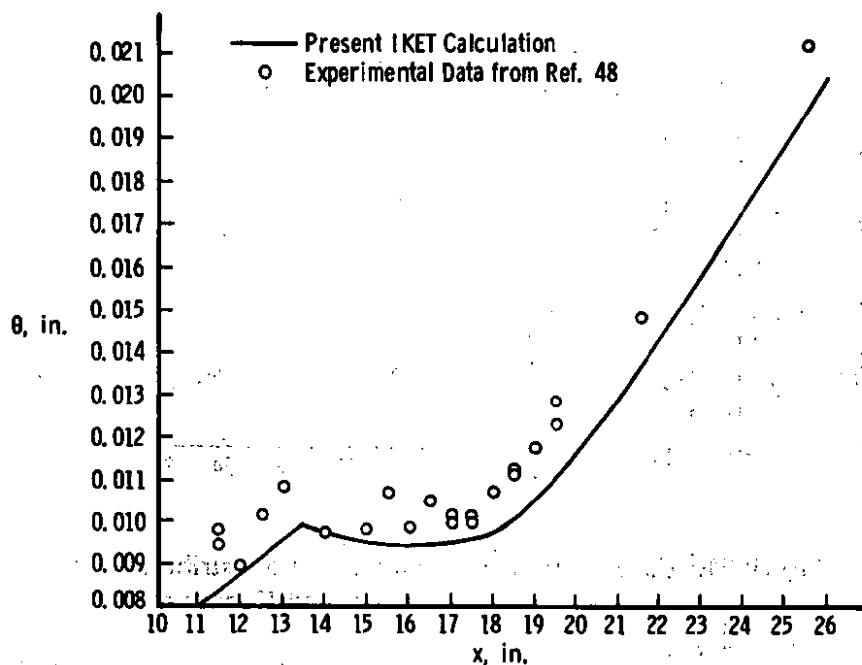
Figure 13. Momentum thickness distribution for hot-wall
condition for Gran, Lewis, and Kubota edge conditions.
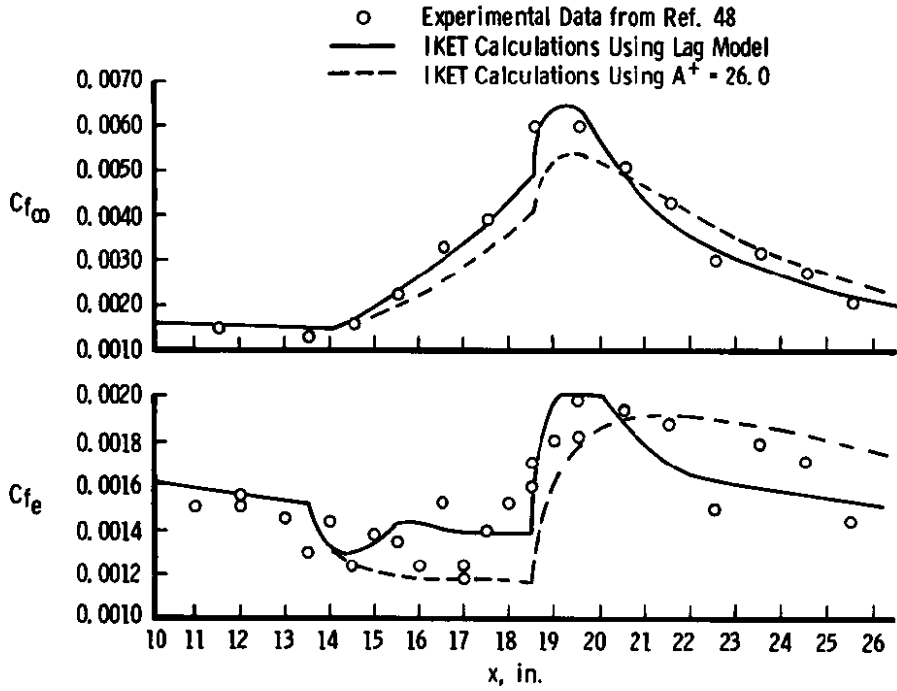
Figure 14. Skin friction distribution for hot-wall condition
for Gran, Lewis, and Kubota edge conditions.
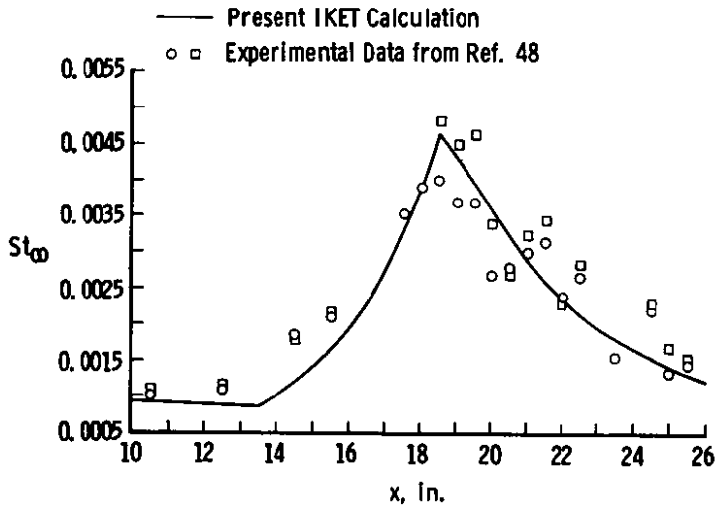
Figure 15. Stanton number distribution for cold-wall condition
using Gran, Lewis, and Kubota edge conditions.

46

respectively. Except for the momentum thickness results, the agreement between the experiment and calculations is reasonably good. As can be seen from Fig. 14, the variation of A_{eff}^{+} with pressure gradient using the lag model discussed earlier resulted in noticeably better IKET calculations than did the assumption of $A_{eff}^{+} = 26.0$ irrespective of the pressure gradient.

Using experimental data as a basis, Johnson and Kaufman (Ref. 50) suggest that the peak heating ratio, H_{pk} (for interaction of shock waves with turbulent boundary layers), can be estimated in terms of the peak pressure ratio, P_{pk}, as

$$H_{pk} = (P_{pk})^{n} \tag{76}$$

where the best hypersonic correlation is achieved by using $n = 0.85$. In Eq. (76), the peak heating ratio, H_{pk}, is defined as the peak heating rate for the interaction flow divided by the heating rate for undisturbed flow at the same location, and the peak pressure ratio, P_{pk}, is defined as the peak $\bar{p}/p_{\infty}$ for the interaction flow divided by $\bar{p}/p_{\infty}$ for the undisturbed flow at the same location. For the present conditions, $P_{pk} = 9.1$ (from Fig. 11), and thus $H_{pk} = 6.53$, which is in good agreement with the results of Fig. 15.

It is germane at this point to examine the variation of the outer-region length scale as computed using the IKET analysis. Figure 16 presents the computed hot- and cold-wall boundary-layer thicknesses and outer-region length scales. The severe adverse and favorable pressure gradients really have little effect on the outer-length scale, and thus the conventional mixing-length turbulent boundary-layer analyses [based on constant outer-length scale, for example $\lambda/\delta = 0.09$ in the Patankar-Spalding (Ref. 10) approach] should yield relatively accurate results

for this condition. Such is indeed the case, as the classical analyses
of Reeves (Ref. 51) and Cebeci and Smith (Ref. 8) report good agreement
with the data of Refs. 47 and 48. In Fig. 16, as in Fig. 9, the ex-
pression $\sqrt{C_\mu^2/2a_t}$ Y/δ represents the ratio of the IKET version of the
conventional mixing-length outer-region length scale to the boundary-
layer thickness.
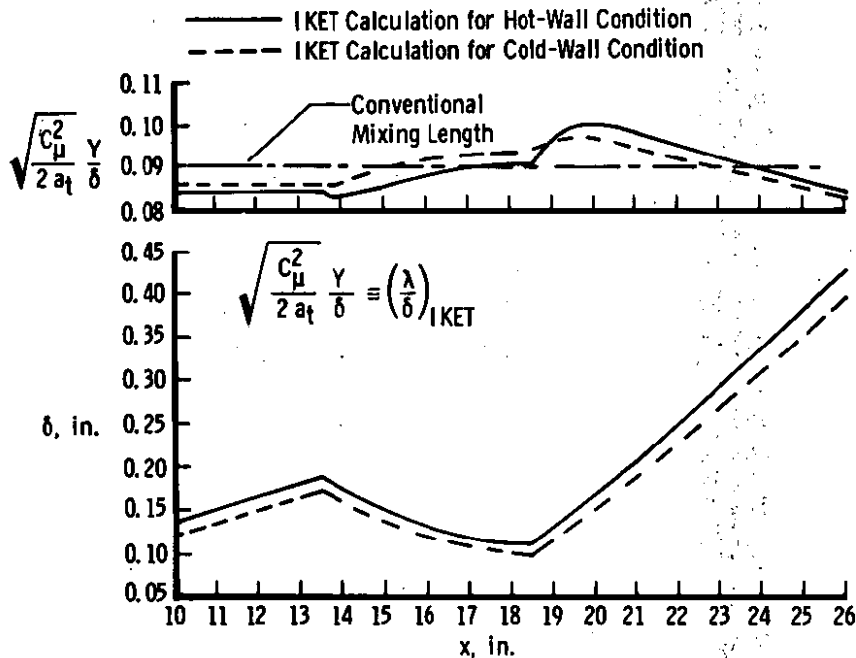
**Figure 16. Outer length and boundary-layer thickness distributions
for Gran, Lewis, and Kubota edge conditions.**

The highly respected kinetic-energy-of-turbulence approach by
Bradshaw and Ferriss (Ref. 21) fails dramatically for this flow situa-
tion. In a later paper Bradshaw (Ref. 52) derived an empirical bulk
compression or dilatation correction formula (essentially an "extra"
strain rate) which, when added to the original analysis, gave good
agreement for the skin friction in the adverse pressure gradient region.
However, this modified approach still failed to adequately predict the
effects of the favorable pressure gradient region.

3.4 COMPRESSIBLE BOUNDARY-LAYER TRANSITION ON A SHARP FLAT PLATE

The comparisons made up to this point have been concerned only with the prediction of turbulent boundary layers. Boundary-layer transition and the transitional predictive aspects of the IKET analysis will now be examined. The classical hypersonic sharp flat-plate boundary-layer transition experiment of Deem, Erickson, and Murphy (Ref. 53) will be used as a comparison. Although results were also obtained from the AEDC-VKF Hypersonic Wind Tunnel (C) and the AEDC-VKF Supersonic Wind Tunnel (A), only the Mach No. 8 AEDC-VKF Hypersonic Wind Tunnel (B) conditions will be considered. The free-stream conditions are

$$M_\infty = 8.09$$
$$Re_\infty/in. = 0.25 \times 10^6$$
$$T_{o,\infty} = 1,325°R$$

with outer-edge conditions

$$M_e = 7.40$$
$$Re_e/in. = 0.235 \times 10^6$$

and a model wall temperature ratio $T_w/T_{o,\infty}$ of 0.80. Transition was experimentally determined based on surface pitot pressure measurements.

The experimental studies of Pate and Schueler (Ref. 54) established that boundary-layer transition on models in supersonic and hypersonic wind tunnels is dominated by radiated aerodynamic noise from the tunnel sidewall turbulent boundary layer. The recent text by Goldstein (Ref. 55) treats on a readable analytical basis the generation and propagation of sound waves for many aerodynamic circumstances. The radiated aerodynamic noise from the supersonic wind tunnel sidewall turbulent boundary layers is normally characterized by the level of the root-mean-square (RMS) radiated pressure fluctuations. Recent measurements by

Laderman (Ref. 56) indicate that for the aforementioned free-stream
conditions the RMS radiated pressure fluctuations in the AEDC-VKF Tunnel
B are approximately 3.5 percent of the free-stream static pressure.
Thus the E term in the IKET equation [Eq. (37)] represents the incident
acoustic energy (in the form of radiated pressure fluctuations) <u>absorbed</u>
by the boundary layer. It is this source term which triggers transition.

The very difficult problem of receptivity as defined by Morkovin
and discussed by Reshotko (Ref. 57) is intimately associated with the
theoretical determination of E. In this analysis E is evaluated via
experimental data, and no effort is made to analytically determine the
absorbed incident acoustic energy by considering the incident spectrum
and its signature within the boundary layer. This is accomplished by
selecting the value of E which places the computed transition point at
the desired location using the appropriate criterion, in this example
the maximum value of the surface pitot measurement. Presented in Figs.
17, 18, and 19 are numerical results from the IKET analysis which were
initiated via a laminar similar solution at the sharp leading edge and
integrated downstream using a constant value for the E source term. The
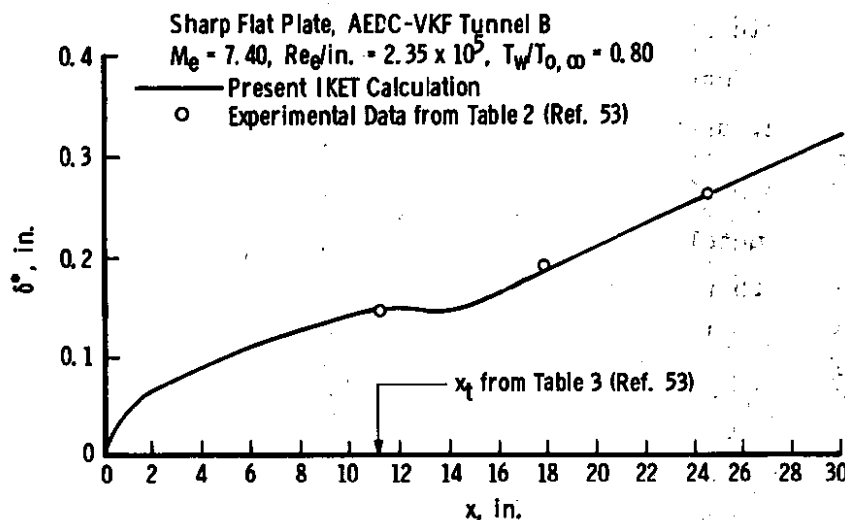
Figure 17. Laminar, transitional, and turbulent displacement
thickness distribution.
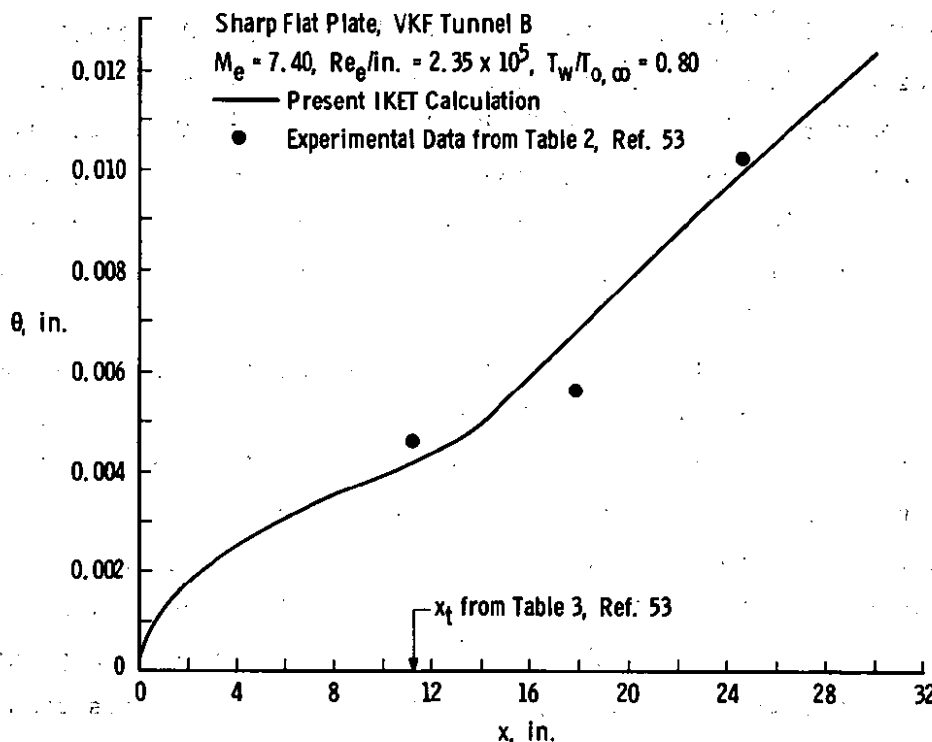
Figure 18. Laminar, transitional, and turbulent momentum thickness distribution.

experimental and computed boundary-layer displacement thicknesses are in good agreement. The transition phenomena are more clearly seen in Fig. 19, where the calculated outer-region length scale starts at zero at the leading edge and increases downstream, reflecting the transition process. At the x = 11-in. station, which is the location of minimum skin friction, the outer-length scale ratio $\sqrt{c_\mu^2/2a_t}$ Y/δ has attained a value of 0.034, which is approximately 40 percent of the maximum value of 0.08, attained when transition to turbulence is complete. Hence, the IKET analysis predicts substantial values of the outer-region length scales before the surface feels any effects of transition. Further discussion of the length scale behavior during transition will be found later in this section.

Also shown in Fig. 19 are IKET-calculated results for cold-wall conditions. The influence of the cold wall is to slightly displace

51

downstream the minimum skin-friction location and the outer length
scale. Hence, the IKET analysis predicts the slight stabilizing effect
of a cold wall on boundary-layer transition. This agrees with the
meager experimental results of Deem et al. (Ref. 53) and with the gen-
erally accepted transition trends [whereas wall cooling stabilizes the
laminar boundary layer relative to transition (Ref. 57)]. The cold-wall
influence on turbulent skin friction (i.e., an increase over the cor-
responding hot-wall value) should also be noted.

Sharp Flat Plate, AEDC-VKF Tunnel B
$M_e = 7.40$, $Re_e/in. = 2.35 \times 10^5$
———— IKET Calculation for $T_w/T_{0,\infty} = 0.80$
– – – – IKET Calculation for $T_w/T_{0,\infty} = 0.40$
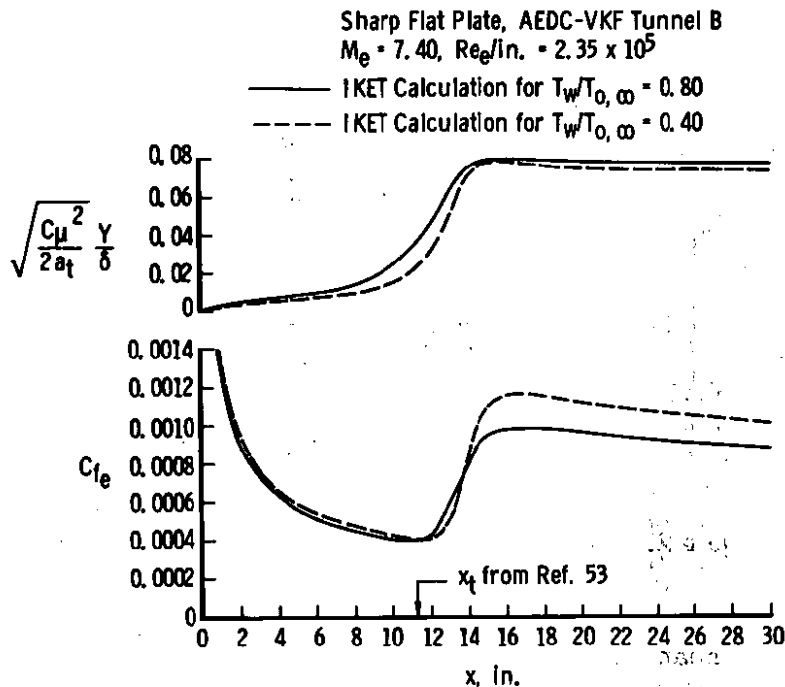
**Figure 19. Laminar, transitional, and turbulent outer
length scale and local skin-friction distributions.**

Any analytical model of the boundary-layer transition process under
hypersonic conditions must include the precursor effect as discussed by
Bushnell and Alston (Ref. 58). This effect is characterized by the
existence of appreciable length scales (i.e., large-scale disturbances)
in the outer region of compressible boundary layers well upstream of the
nominally accepted transition location. Figure 20, taken from Ref. 58,
schematically illustrates the phenomenology of the precursor effect.

Location x_1 indicates the point of the initial breakdown of laminar flow. At this location laminar profiles and characteristics prevail. Location x_2 represents the point at which turbulent bursts are initiated in the outer region of the still laminar boundary layer and the point at which appreciable growth of the outer-region length scales begins. The location at which transition is indicated by surface measurables such as skin friction and heat transfer is represented by x_t. Since turbulent bursts are observed far upstream of the conventional transition location
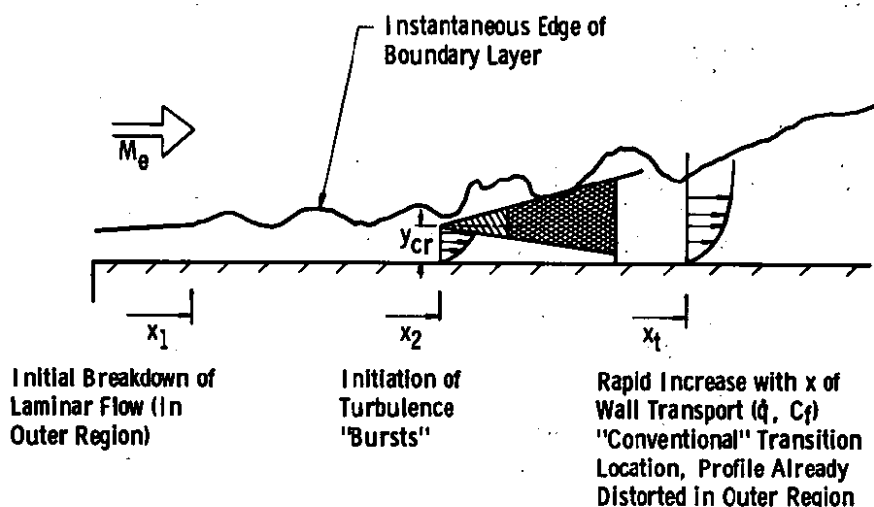
Figure 20. Schematic of the precursor effect in hypersonic boundary-layer transition.

where the wall heat transfer or skin friction deviates from the laminar values, transition at hypersonic speeds must occur initially away from the wall as per the work of Potter and Whitfield (Ref. 59) and Stainback (Ref. 60). Thus, the outer portion of the mean flow profiles may already be distorted by turbulence effects at the conventional transition location. This was shown by Fischer and Weinstein (Ref. 61) and is contrary to the usual numerical approach, e.g., Adams (Ref. 62), Harris (Ref. 63), and Kuhn (Ref. 64), where the intermittency distribution is anchored to the conventional transition location with a fully laminar profile. This precursor effect is predicted properly by the IKET analysis as shown in Fig. 21, which gives the turbulent shear

stress profiles for three streamwise locations along the plate, namely 6, 12, and 18 in. The IKET analysis predicts at the 6-in. location, which is far upstream of the surface-indicated transition location, a sharp "spike" in the turbulent shear stress near the outer edge of the boundary layer. The transitional turbulent shear stress profile at x = 12 in. approaches the fully turbulent value at the x = 24-in. location, especially for the hot-wall condition. Thus, in the outer region of the boundary layer at x = 12 in. the flow is turbulent, and hence the outer portions of the boundary-layer mean flow profiles are indeed distorted by upstream turbulence effects.
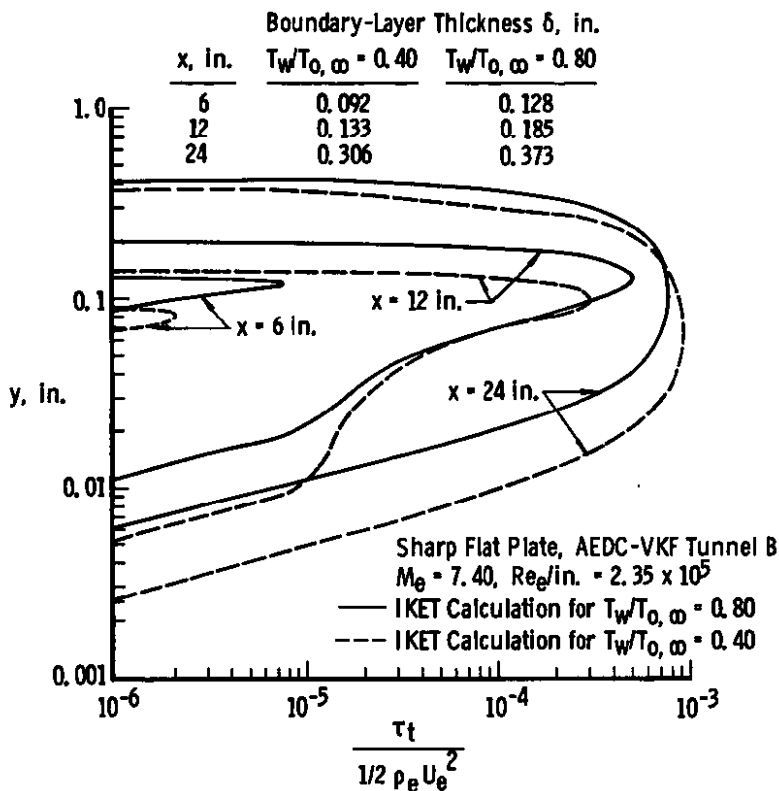
Figure 21. Turbulent shear stress profiles as an indicator of the precursor effect.

Defining the distance y_{cr} shown in Fig. 20 as the y location where the turbulent shear stress attains its maximum value allows the results of Fig. 21 for the x = 6-in. location to be tabulated as

$T_w/T_{0,\infty}$	y_{cr}/δ
0.40	0.89
0.80	0.92

which is in good agreement with the results of Potter and Whitfield (Ref. 59) and Stainback (Ref. 60). Since the value of the maximum turbulent shear stress at x = 6 in. is approximately one percent of the maximum turbulent shear stress at x = 12 in., it is reasonable to postulate that the IKET-calculated concentration of turbulent shear stress near the edge of the boundary layer represents in a time-mean sense the turbulent "burst" observed experimentally by Potter and Whitfield (Ref. 59) as well as by Fischer and Weinstein (Ref. 61).

The edge Mach number for this calculation was 7.40, a low hypersonic Mach number which exceeds the formal limit of validity of Morkovin's hypothesis (Ref. 27). Nevertheless, the results of the computations for this example appear satisfactory, indicating that, at the formal limit of validity, "breakdown" is slow rather than catastrophic. The Morkovin hypothesis as used in this analysis permits structural constants as deduced from incompressible turbulent flow to be used for edge Mach numbers up to about five. Thus, for the edge Mach number (7.40) used in this example, some turbulence model constants may in reality deviate slightly from the assumed values, but any deviation must be very gradual at this low hypersonic Mach number, and the resulting impact upon the calculations must be correspondingly small.

Figure 19 also indicates that the outer region length scale ratio expressed as $\sqrt{c_\mu^2/2a_t}$ Y/δ possesses a value near 0.08. The usual assumption made in mixing-length hypotheses is that the outer-region length scale ratio, λ/δ, has a value of 0.09. Previous examples considered in this report have tended to confirm the value of 0.09. This

example raises the possibility that for hypersonic flows the outer-region length scale ratio may decrease from the usually accepted value of 0.09.

The determination of the incident acoustic energy, E, absorbed by the boundary layer is greatly facilitated by the use of IKET-generated plots, of which Fig. 22 is illustrative. This figure presents the relationship between $Re_{e,xt}$, the edge Reynolds number at transition, and $\bar{E}_e$, the incident absorbed acoustic energy made dimensionless by $\rho_e U_e^3$. For the sharp flat plate at a given Mach number and wall temperature, these parameters collapse all free-stream Reynolds numbers and values of E onto a single curve which is a straight line when displayed on a log-log plot. Thus, the absorbed incident acoustic energy required for transition at a given location can be readily ascertained. Implicit in this procedure for obtaining the required incident acoustic energy absorbed by the boundary layer, E, is that the receptivity be handled in an "effective" manner. Linear compressible stability theory as developed by Mack (Ref. 65) can be used to examine qualitatively the problems inherent in the theoretical calculations of E. The results of Mack for a flat plate, as reported by Reshotko (Ref. 57), show that in the Mach number range from 2.5 to 7 all sound frequencies grow rapidly monotonically from the leading edge, thus indicating that the acoustic energy absorbed by the transitioning boundary layer is a function of the RMS radiated pressure fluctuations. Above a Mach number of about seven the laminar boundary layer becomes much more selective, and only disturbances of discrete frequencies are amplified. This leads to behavior in which the energy absorbed by the boundary layer is dependent upon both the disturbance environment spectral energy distribution and the detailed structure of the boundary layer. The value of E as determined from graphs, of which Fig. 22 is typical, implicitly contains all the nuances of receptivity for a single given case. Nothing additional about E in general can be inferred.
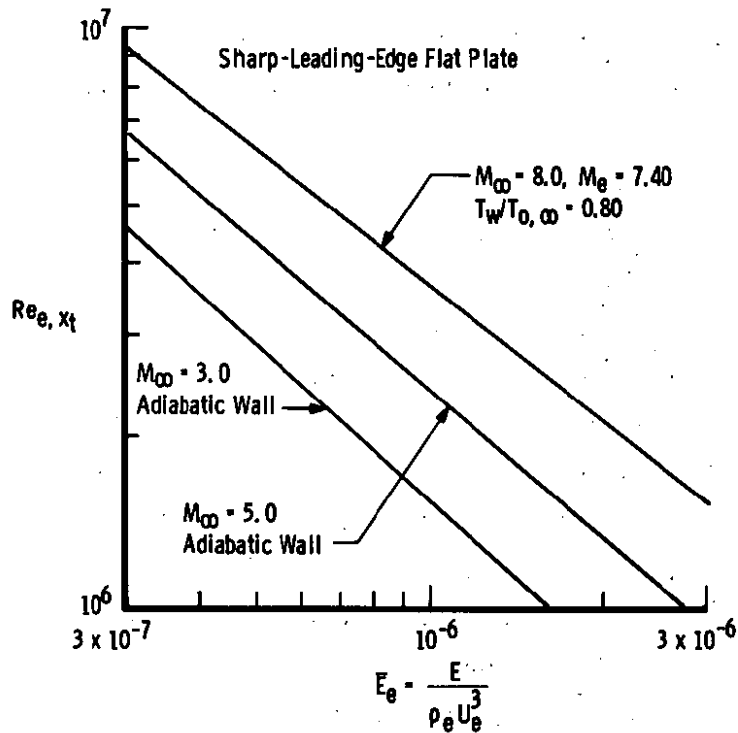
Figure 22. Transition Reynolds number versus absorbed
acoustic energy for a sharp-leading-edge flat plate.

3.5 COMPRESSIBLE BOUNDARY-LAYER TRANSITION ON A SHARP CONE

The first IKET analysis and results for axisymmetric boundary layer on bodies of revolution will be for sharp cones. The same turbulence model may be used in IKET analysis of axisymmetric boundary layers as was used in the IKET analysis of planar boundary layers. Presented in Fig. 23 are sharp-cone transition Reynolds numbers (based on edge conditions) versus dimensionless incident absorbed acoustic energy, $\bar{E}_e$. The results shown in Fig. 23 for sharp cones are very reminiscent of the results portrayed in Fig. 22 for sharp flat plates.

The results of Pate (Ref. 66) for sharp, slender cones show that the ratio of the cone transition Reynolds number to the planar transition Reynolds number varies from about 2.5 at a Mach number of 3.0 to

57
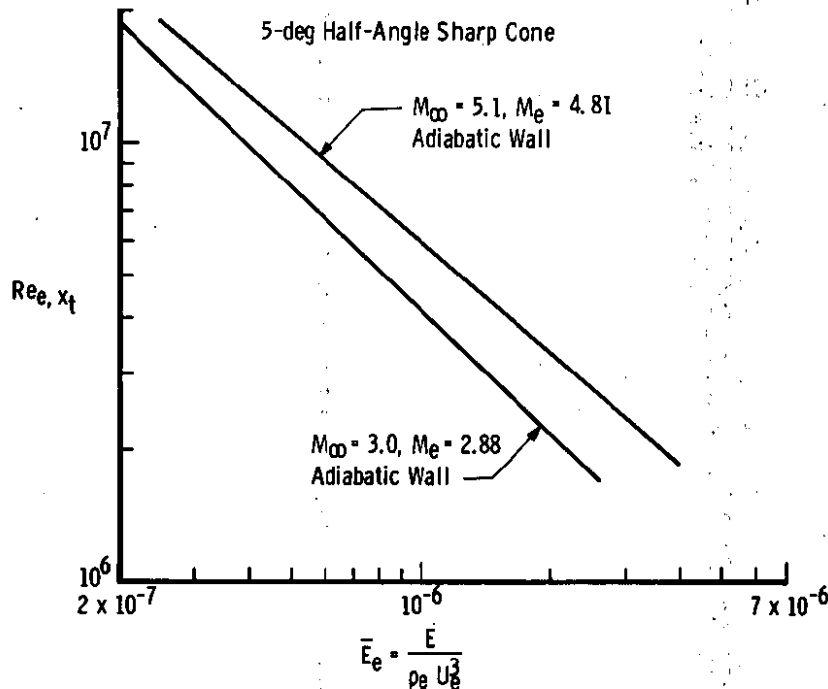
Figure 23. Transition Reynolds number versus absorbed acoustic energy for a sharp cone.

approximately 1.0 at a Mach number of 8.0. These results (taken from Fig. 11 and Table 3 of Ref. 66) are reproduced in Fig. 24, where the legend delineates the meaning of the open, solid, and flagged symbols. The solid line in Fig. 24 represents the IKET-predicted transition Reynolds number ratios as a function of the edge Mach number. The solid line was generated using identical edge conditions for the sharp cone and the flat plate and identical values of the absorbed incident acoustic energy, E. The results of Fig. 24 suggest that the acoustic energy absorbed by both a sharp-cone and a flat-plate boundary layer (both with the same edge conditions) must be the same.

Deviations begin to appear at a Mach number of about six, which is near the limit of validity of Morkovin's hypothesis (Ref. 27). As discussed in Section 3.4, the formal range of validity of some turbulence model constants has probably been exceeded by Mach number six, but

the rather drastic departure of the IKET-predicted results for the higher Mach numbers is not indicative of what must be a rather gradual breakdown in the turbulence model. Moreover, previous calculations reported herein have indicated reasonable results for low hypersonic Mach numbers. Linear compressible stability theory offers a possible explanation for the anomaly observed in Fig. 24. As pointed out in Section 3.4, linear compressible stability theory indicates that above a Mach number of about 7 (for flat plates at least) the laminar boundary layer becomes selective in the frequency of disturbances amplified. The IKET analysis as applied in this example has essentially assumed energy absorption on an RMS basis (i.e., for given edge conditions, E values for both planar and conical flows were taken to be the same). However,
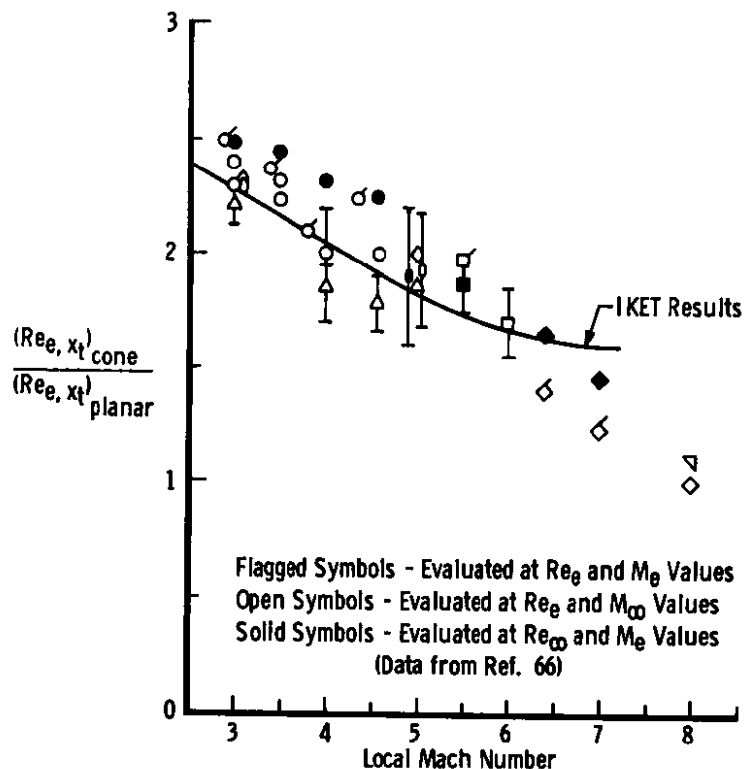
Figure 24. Cone and planar transition Reynolds number ratios as a function of local Mach number.

in regions where the growth of disturbances is highly dependent upon disturbance frequency and detailed boundary-layer structure, a broadband representation such as this should not be successful. Differing receptivities of planar and conical boundary layers at the higher Mach numbers then provide a reasonable explanation of the anomaly observed at higher Mach numbers in Fig. 24. An interesting discussion of the relationship between linear stability theory on a cone and a flat plate is given by Mack (Ref. 65).

Previous results discussed have established the relationship between the transition location and the absorbed incident acoustic energy, but no mention has been made of the effects (if any) of absorbed incident acoustic energy upon turbulent boundary layers. The results presented in Fig. 25 show the effect of various energy absorptions upon the IKET-computed skin friction for typical wind tunnel flow conditions
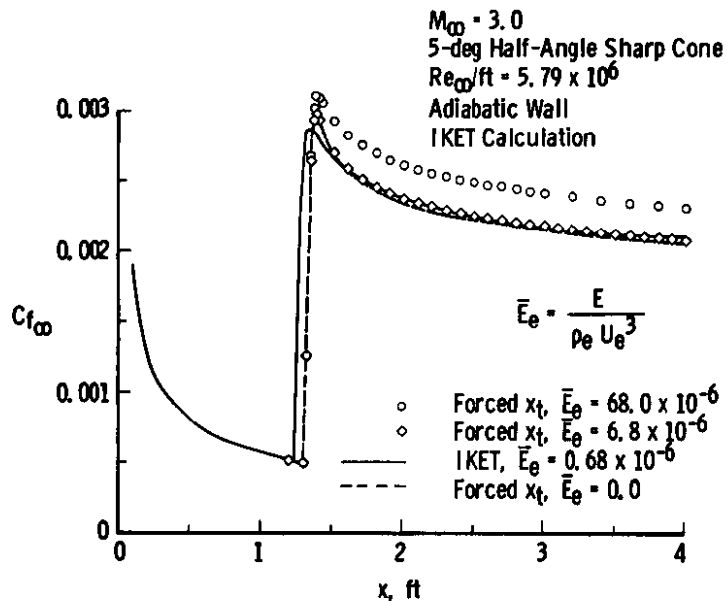
Figure 25. Effect of acoustic energy absorption on a turbulent boundary layer.

over a 5-deg half-angle sharp cone. The solid line in the figure was
calculated using the usual IKET transition analysis, in which an acous-
tic energy absorption is specified and the resulting transition process
is calculated; the dashed line was computed by forcing transition to
occur instantaneously with no energy absorption; the symbols were
computed using forced instantaneous transition and values of energy
absorption 10 and 100 times that required for the transition calcula-
tion. A decade increase in the energy absorption has almost no dis-
cernible effect upon the calculated skin friction, whereas the large
multiple of 100 gives about 10 percent increase above the other cal-
culations. This latter amount represents almost total absorption of all
acoustic energy incident upon the boundary layer and hence can be con-
sidered an unrealistic number. Thus, for typical calculations the
effect of absorbed acoustic energy upon turbulent boundary layers is
small. It can therefore be inferred that in typical supersonic wind
tunnels the acoustic environment has considerable effect upon the transi-
tion location but little effect upon the turbulence level in a fully
turbulent boundary layer.

3.6 SURFACE ROUGHNESS IN PLANAR COMPRESSIBLE TURBULENT BOUNDARY LAYERS

Roughness effects were investigated using as a basis of comparison
the results of Reda, Ketter, and Fan (Ref. 37), which were taken on the
flat nozzle wall of a supersonic nozzle in which the wall opposite was
contoured. A wide variety of roughness conditions was studied over a
wide range of free-stream Reynolds numbers. Skin-friction and profile
data were taken, with the skin-friction data being obtained from a
floating balance. Examined in this report are the data for smooth
walls and sand grain roughness of 80, 50, and 24 grit. This range of
roughness allows all three regimes of rough-wall turbulent boundary-
layer flow to be examined.

Figure 26 contains a summary of the predictive ability of the rough-wall IKET analysis. The smooth-wall computed results and experimental data show the same trend with increasing Reynolds numbers, but the predicted level is slightly low. This is difficult to explain but not too disturbing, as changes in free-stream conditions and/or the location of the boundary layer's virtual origin in the computed results or sensitivity of the balance in the experiment could have caused such an error. The 80-grit data are quite interesting in that initially the roughness Reynolds number was very close to the "smooth" limit; hence,
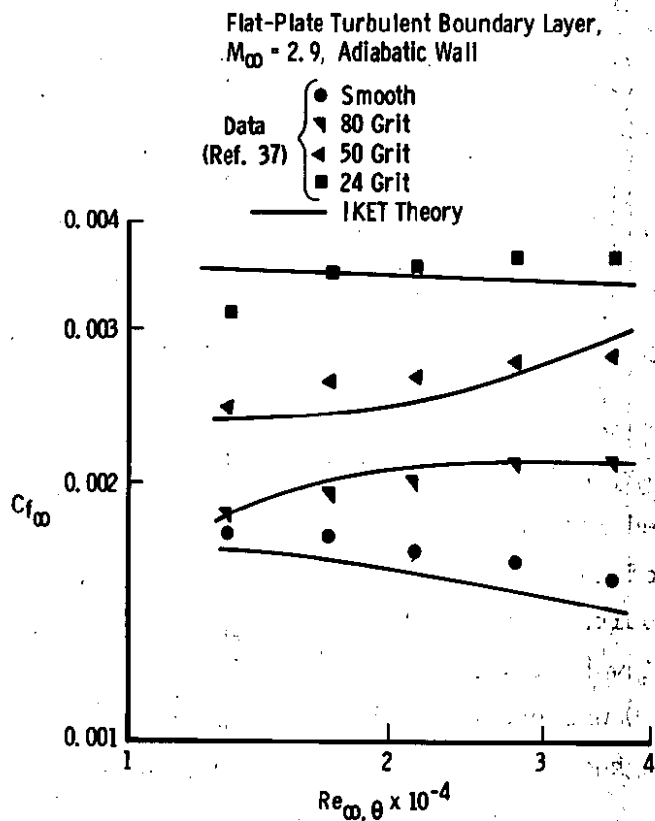
Figure 26. Skin friction versus $Re_{\infty,\theta}$ for rough-wall flow.

the resulting nearly smooth-wall value of skin friction. As the Reynolds number increased, the roughness became more pronounced with respect to the viscous sublayer, causing a thinning which is reflected in the higher value of skin friction. The 80-grit roughness remained

continuously in the transitional roughness regime, thus allowing the Healzer et al. (Ref. 30) approach (see Section 2.4) to be used. The 50-grit roughness was more difficult, as at the low free-stream Reynolds numbers the roughness was transitional, and at higher free-stream Reynolds numbers the roughness was fully rough. The fully rough regime was treated using the approach of Finson (Ref. 33., see Section 2.4). The fully rough calculations used the suggestion of Finson that sand grain results could be adequately predicted, assuming hemispherical roughness elements of a height characteristic of the grit specification (0.00225 ft for 24-grit, for example) and a center-to-center spacing of two element diameters. The results obtained were considered satisfactory, and no computer experiment was undertaken to examine various configurations of roughness element shape and spacing. The 24-grit sand grain roughness was large enough so that the viscous sublayer was completely destroyed at all the free-stream Reynolds numbers of interest, and the flow was fully rough, thus allowing the Finson approach to be used for all Reynolds numbers.

For some free-stream conditions the roughness was such that the flow was initially fully rough, but as the viscous sublayer thickened, the flow reverted into the transitional regime. No completely satisfactory method of interfacing the fully rough/transitional regimes was evolved, but results appeared reasonable if the Finson fully rough analysis, once invoked, was used until a local roughness Reynolds number below 40.0 was encountered. The Healzer et al. (Ref. 30) transitional roughness analysis was then applied.

3.7 ROUGH-WALL HEMISPHERE-CYLINDER IN HYPERSONIC FLOW

Hemisphere-cylinders have traditionally been used as standardized test shapes in supersonic and hypersonic aerodynamics because they offer a wide range of edge pressures, edge temperatures, and pressure gradients.

Recently the AEDC-VKF Hypervelocity Wind Tunnel (F), which uses nitrogen as a working medium, was used to investigate the effectiveness of sand blasting model surfaces in order to induce turbulent flow. A hemisphere-cylinder model with a nose radius of 2.5 in. was instrumented with heat-transfer gages and sand blasted over one sextile as shown in Fig. 27. Typical run conditions in Tunnel F were as follows:

$$M_\infty = 9.0$$
$$Re_\infty/ft = 3.40 \times 10^6 \text{ to } 5.85 \times 10^6$$
$$T_\infty = 191°R$$
$$T_w = 540°R$$
$$\text{Nitrogen}$$

3.5-mil Roughness, ±30 deg about the ø = 180-deg Ray

3.5-mil Roughness Begins 0.5 in. from Model Stagnation Point (x/R_N = 0.20)
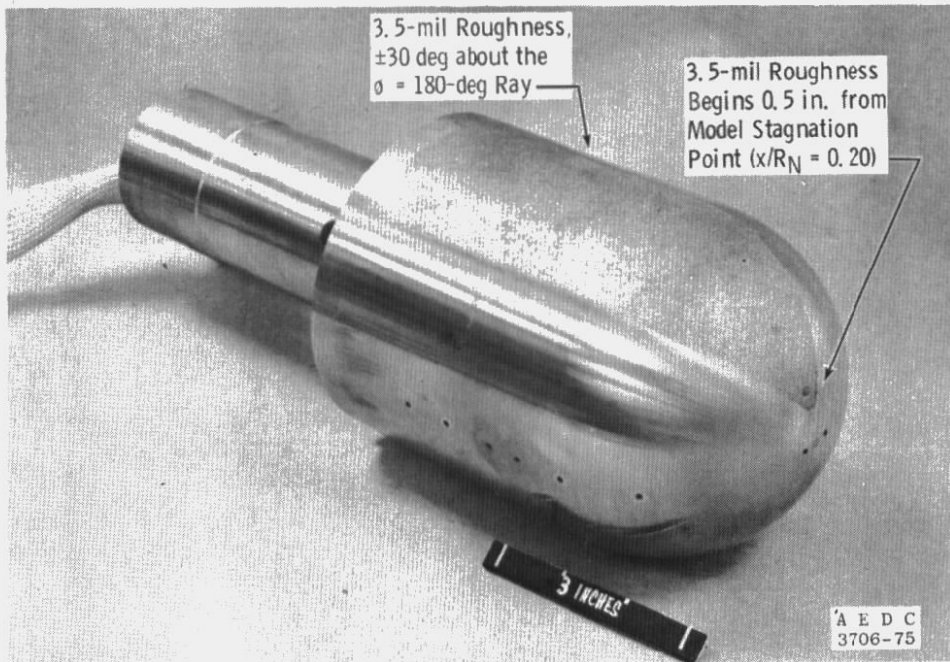
Figure 27. Tunnel F rough-wall hemisphere-cylinder model.

Figure 28 presents experimental heat-transfer data for the test conditions delineated above. The solid symbols represent data taken on the sand-blasted sextile of the model, whereas the open symbols represent

data taken on the "smooth" portion of the model. For reference, theo-
retical computations made for laminar flow and for fully turbulent flow
using a conventional mixing-length approach (BLIMP, Ref. 67) are shown.
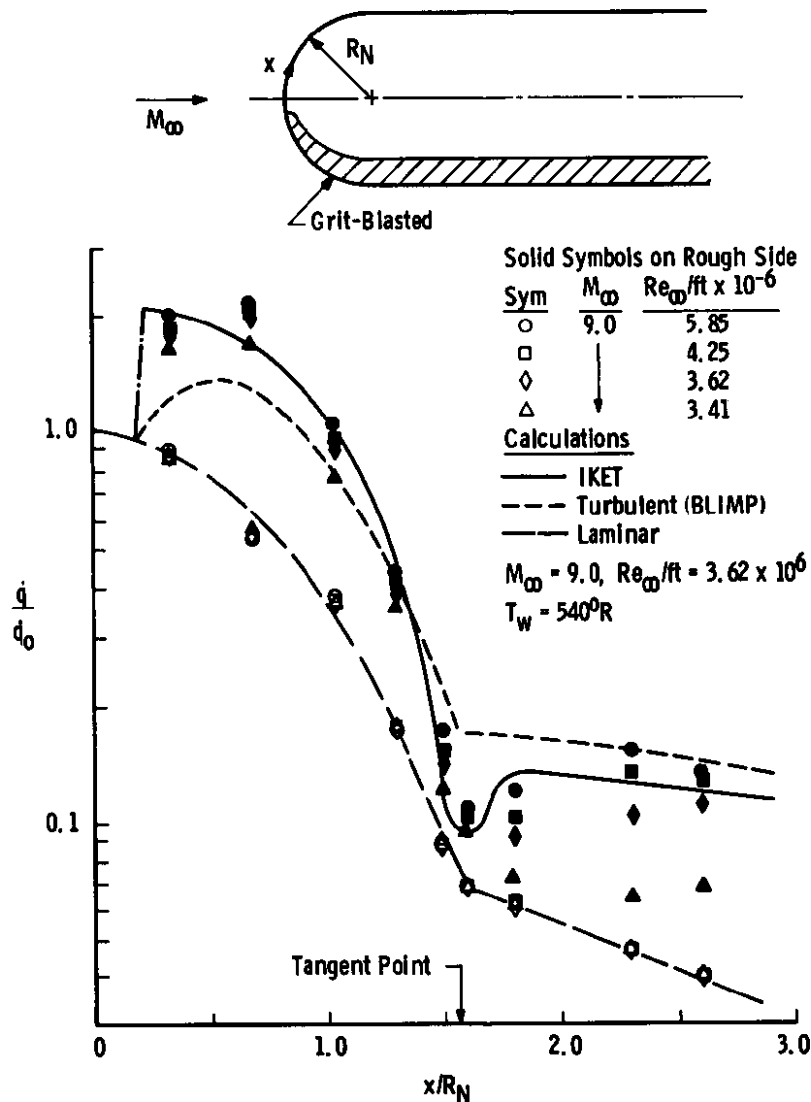
**Figure 28. Rough-wall hemisphere-cylinder in
hypersonic flow.**

The experimental data initially indicate heat-transfer rates in excess
of the fully turbulent calculations. The discrepancy is caused by the
enhanced heat-transfer rate to the rough surface, an effect not accounted
for in the fully turbulent BLIMP calculations. The real region of

interest occurs, however, between the $x/R_N = 1.0$ and $x/R_N = 1.5$ stations. In this region the measured heat-transfer rates drop below the predicted fully turbulent values and approach the laminar predicted values. Thus the data indicate that relaminarization, or something closely akin, is occuring in this region. Figure 29 shows the edge pressure ratio $(\bar{p}/p_\infty)$, the edge Mach number (M_e), and the acceleration parameter K [defined by Eq. (74)] as computed using the AEDC version of the NASA Ames characteristics computer code (Ref. 68) with the nose solution generated by the Aungier program (Ref. 69). Near the $x/R_N = 1.5$ location, K increases dramatically to a value near 1×10^{-6}. The local maximum value of K at this location indicates that according to the criterion of Fig. 8, relaminarization is just possible irrespective of $Re_{e,\theta}$. Actually the K value falls so close to the threshold boundary indicated in Fig. 8 that it is difficult to assess its meaning; i.e., relaminarization may or may not take place. In spite of the high values of K near the $x/R_N = 0.5$ region, relaminarization did not occur, as roughness effects were dominant. Calculations were made for this model in which a smooth-wall flow was tripped turbulent initially and then computed downstream from that location using the IKET analysis. Relaminarization with the attendant approach of $\sqrt{C_\mu^2/2a_t}$ Y/δ to near-zero values was always observed prior to $x/R_N = 0.25$. Therefore, the presence of roughness can alter the threshold boundary for relaminarization as shown in Fig. 8. Of course relaminarization could still occur at x/R_N near 1.50 since k_r/δ decreases from 0.2 near the $x/R_N = 0.5$ location to 0.02 near the $x/R_N = 1.50$ location, indicating that the relative roughness has decreased by an order of magnitude.

Figure 28 presents the results of the IKET rough-wall analysis for the conditions of Fig. 29. The IKET analysis with E, the incident acoustic energy absorbed by the boundary layer, taken as zero effectively and realistically computes both the roughness-induced heat-transfer augumentation in the $x/R_N = 0.5$ region and the relaminarization-like process near the $x/R_N = 1.5$ region. The least pleasing result

is observed near the $x/R_N = 1.80$ station, where the predicted heat-transfer ratio is somewhat above the measured values. No explanation is apparent, as the remainder of the cylindrical portion is adequately predicted. Fig. 30 reveals a most intriguing result, namely that the
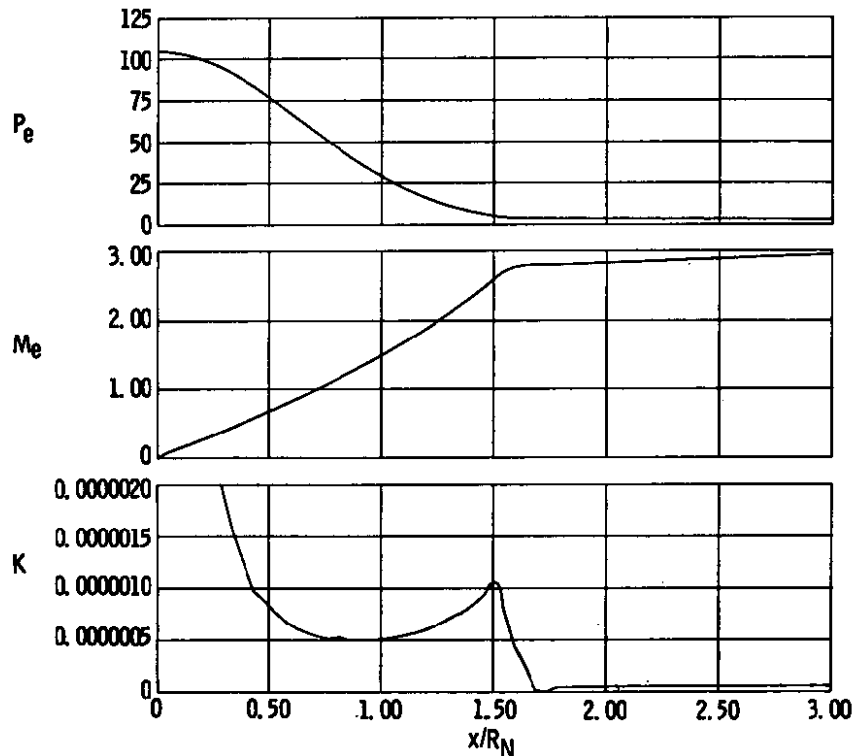
Figure 29. Edge conditions and acceleration parameter for
$M_\infty = 9$ hemisphere-cylinder.

outer-region length scale $\sqrt{c_\mu^2/2a_t}$ Y/δ exhibits <u>turbulent</u>, not <u>laminar</u> behavior. Thus, relaminarization in the sense of the example in Section 3.2 did not occur near the $x/R_N = 1.5$ region of the hypersonic rough-wall hemisphere-cylinder. Additional computations were made in which the baseline turbulence model values of the parameters κ and A_{eff}^+ were assumed. These computations showed no laminar-like behavior in the heat-transfer rate about the $x/R_N = 1.5$ region. Hence, the IKET analysis indicates that the laminar-like behavior observed near $x/R_N = 1.50$ in the rough-wall hemisphere-cylinder data from Tunnel F is caused not

by a reversion to laminar flow but by the acceleration (large favorable pressure gradient)-induced growth of the viscous sublayer. The value of A^+_{eff}, which is a measure of the viscous sublayer thickness (see Section 2.4), is computed to be as large as 40 in the region of interest. This represents a very large increase in the effective thickness of the viscous sublayer, as A^+_{eff} was small near the fully rough/transitional roughness interface. The interpretation of Kays and Moffat (Ref. 29),
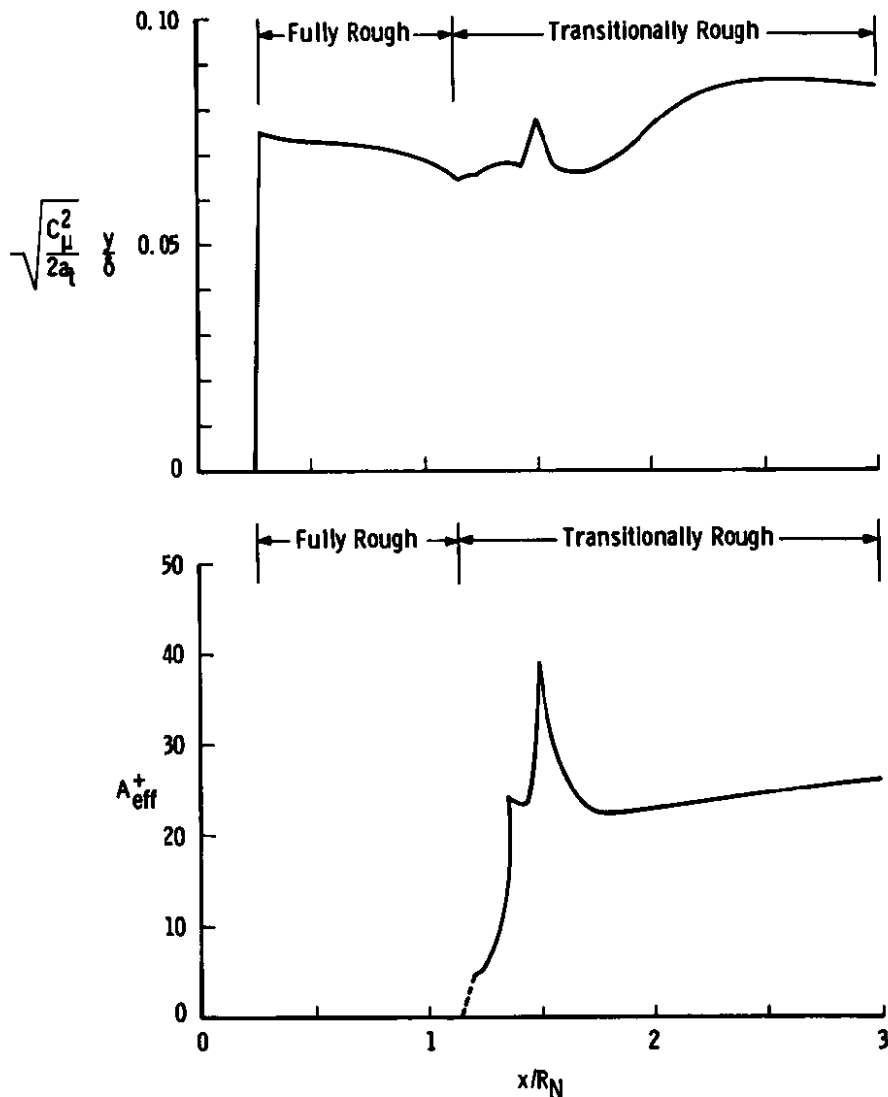
Figure 30. Hypersonic hemisphere-cylinder outer region length scale and A^+_{eff} distributions.

AEDC-TR-77-96

in which relaminarization is attributed to the viscous sublayer's
overwhelming the remainder of the boundary layer (very large
values of A_{eff}^{+}), thus suggests that the favorable pressure gradient in
the proximity of x/R_N = 1.50 was not strong enough to result in a vis-
cous sublayer thickness approaching the boundary-layer thickness.
Because the viscous sublayer thickness remained relatively thin ($A_{eff}^{+} \approx$
40), the outer-region length scale as computed using the IKET analysis
did not show any tendency to approach zero. Hence at the x/R_N = 1.50
region the flow could be viewed as verging on relaminarization. The K
value of near 1 x 10^{-6} and the IKET-computed value of $Re_{e,\theta}$ of 700 at
x/R_N = 1.5 fall so close to the threshold curve as given in Fig. 8 that
the conclusion of impending relaminarization is reinforced.

The outer-region length scale ratio as shown in Fig. 30 never
exceeds a value of 0.086 and appears to be approaching a value of 0.080.
As in previous low hypersonic examples (Section 3.4) the outer-region
length scale ratio is less than the usually accepted 0.09. The work of
Bushnell, Cary, and Holley (Ref. 70) established that the value of the
outer-region length scale ratio, λ/δ, is dependent upon the Reynolds
number, with the value of the ratio increasing dramatically for low
Reynolds number flows. The IKET-computed values of the outer-region
length scale ratios for the low Mach number hypersonic flows suggest
that the ratio may also be a function of the Mach number. In their
discussion of the outer-region length scale ratio, Bushnell, Cary, and
Harris (Ref. 9) ascribe to this ratio a value independent of the Mach
number, citing the results of Maise and McDonald (Ref. 71). The data
examined by Maise and McDonald covered a Mach number range from zero to
five and confirmed Morkovin's hypothesis concerning the structure of
compressible turbulent boundary layers for this Mach number range.
These data say nothing about the behavior of the outer-region length
scale ratio at Mach numbers above five. However, the data of Horstman
and Owen (Ref. 72) taken on the cylindrical portion of a cone-ogive-
cylinder at a free-stream Mach number of 7.2 exhibit values of the

outer-region length scale ratio in the range from 0.06 to 0.07. Thus
the behavior of this ratio at high Mach numbers is an open question.
From the results of this analysis it is not possible to ascertain
explicitly whether this ratio is decreasing in the low-hypersonic regime
or whether the decrease is fortuituously being caused by the assumption
that all structural constants are invariant with Mach number. The
results of the IKET analysis as well as the experimental data of Horst-
man and Owen (Ref. 72) do indicate that such a dependence upon Mach
number in the low-hypersonic regions may be present and significant.
More experimental work on turbulent boundary-layer structure is required
to settle the question of the behavior of the outer-region length scale
at elevated Mach numbers.

The roughness element geometry produced by sand blasting the wind-
tunnel model is of a very different nature from the sand grain roughness
for which the turbulence model is postulated. The results of Dirling
(Ref. 36) as presented in Fig. 3 provide a correlation between any
roughness [with some restrictions as suggested by Reda, et al. (Ref. 37)]
and sand grain roughness. The sand-blasted roughness observed via
enlarged photographs of sample cross sections is random. Because of
this randomness the parameters needed to utilize the correlation in Fig.
3 were at least averages and only approximate. Nonetheless, the corre-
lation of Fig. 3 provided an estimate of the effective sand grain rough-
ness size. The Dirling correlation showed the effective sand grain
size, k_r, to measured profilometer mean height, k_a, to be about 0.5 to
1.0. In the IKET calculations presented in this section a value of $k_r =$
0.0002 ft was used, as the measured k_a was 3.5 mil (0.000292 ft) and
0.0002 was a reasonable mean. The IKET calculations exhibited little
sensitivity to k_r if k_r was of sufficient magnitude to result in fully
rough flow initially. It was also found that transition could be
induced by roughness effects for $x/R_N < 0.25$ and that, whether induced
by roughness or tripped, the behaviors of the heat-transfer rate for

$x/R_N > 0.25$ were essentially the same. This calculation illustrates some of the extent of the physics embodied in the IKET extended mixing-length analysis.

3.8 COMPRESSIBLE TURBULENT BOUNDARY LAYERS WITH TRANSPIRATION

Ablation, which often occurs on hypersonic vehicles, especially during reentry, is usually simulated in ground test facilities by transpiration (i.e., blowing). Thus an assessment of the ability of this analysis to accurately predict transpired flows is in order. The form of the IKET equation as given by Eq. (16) can be used to determine the changes, if any, that must be made to Eq. (37), the IKET equation used in this analysis, to account for transpiration effects. Only the quantities evaluated at the surface (y = 0) must be examined, as the integral terms explicitly contain $\bar{v}$ in an acceptable, consistent form as do the edge (y = δ) expressions. The expression $\overline{q^2}$ appears as a multiplier in every one of the quantities to be examined except $\overline{p'v'}$ and $\overline{(v')^2}$. At the surface $\overline{q^2}$ and v' are identically zero since turbulent motion is completely damped at the wall. Thus transpiration adds no terms to the IKET equation as given by Eq. (37) - as long as the transpiration-induced velocity perturbation, v'_w, is taken to be identically zero. Thus the additional assumption that the transpiration flow is laminar at the wall is herein invoked, i.e., $v'_w = 0$.

The data of Squire (Refs. 73 and 74), taken at nominal Mach numbers of 1.8, 2.5, and 3.6, were used as the basis for examining the IKET analysis transpiration results. These data were taken in a blowdown supersonic wind tunnel, with a sintered bronze plate used as the porous wall. Velocity profiles were measured at a number of stations, and skin-friction coefficients were deduced by means of the momentum integral equation and the measured profiles. Nominal test conditions for the data presented by Squire are given in Table 2.

Table 2. Test Conditions for Squire's Data

Mach Number	$P_{o,\infty}$, psi	$T_{o,\infty}$, °R	Re_∞/ft	$(\overline{\rho v})_w / (\rho U)_e$
1.8	26.7	527.4	8×10^6	0.0013
2.5	44.7	527.4	9.7×10^6	0.0013
3.6	119.7	529.2	15.1×10^6	0.00065

The IKET analysis was applied by placing the virtual origin for the calculations to match the values of the momentum and displacement thicknesses measured for the untranspired case at the first station where profiles were reported by Squire. Once the location of the virtual origin for a given Mach number was obtained, it was considered invariant with the blowing rate:

$$B = \frac{(\overline{\rho v})_w}{(\rho U)_e} \tag{77}$$

Presented in Fig. 31 for nominal Mach numbers of 1.8 and 2.5 are typical measured velocity profiles (Squire), velocity profiles computed using the IKET analysis, and velocity profiles as calculated by Pletcher (Ref. 75) using a conventional mixing-length approach. Agreement between the measured and IKET-computed profiles is satisfactory. The calculations of Pletcher show some discrepancies when compared with the experimental profiles. Calculations were also made using the computer code developed for this analysis operating in a conventional mixing-length mode (i.e., λ/δ forced to be 0.09). Typical points from this calculation are shown by an asterisk (*) in Fig. 31. The points fall directly upon the results presented by Pletcher, thus indicating the importance of the outer-region length scales for transpired flows. Figure 32, which presents $\sqrt{C_\mu^2/2a_t}$ Y/δ and B as functions of distance down the plate illustrates the effect of using an extended mixing-length formulation. In the region where transpiration is occuring, the outer-region length

scale decreases monotonically from the expected value of 0.09 to about 0.08. The velocity profiles (as shown in Fig. 31) generated with the IKET analysis confirm the effects of this decrease.
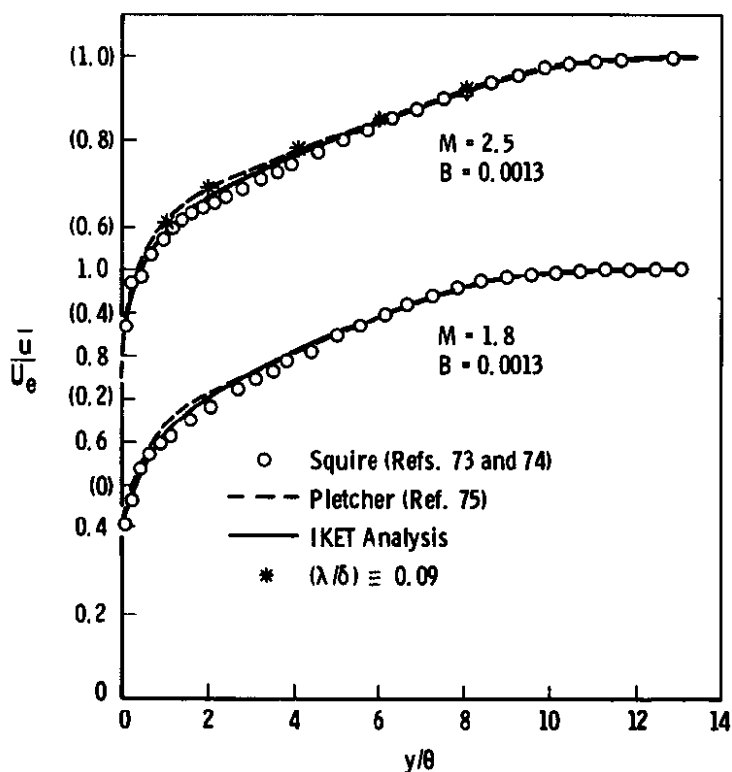
Figure 31. Transpired velocity profiles of Squire.

The skin-friction coefficients as deduced by Squire, calculated by the present method, and computed by Pletcher are presented in Table 3.

Table 3. Skin Friction Coefficients for Squire's Data

M_∞	C_f-IKET	C_f-Pletcher[a]	C_f-Squire[b]	B
1.8	0.001408	0.00126	0.00140	0.00130
2.5	0.001057	0.00092	0.00100	0.00130
3.6	0.00096	--	0.00099	0.00065

[a]Ref. 75

[b]Refs. 73 and 74

Table 3 indicates that the IKET analysis overpredicts by a slight amount the values indicated by Squire and that Pletcher consistently underpredicts the values indicated by Squire. Actually, both the IKET predictions and the Pletcher predictions of skin friction are within the accuracy quoted by Squire. Nevertheless, the IKET-predicted skin friction coefficients deviate less from the experimental values than do the values given by Pletcher.
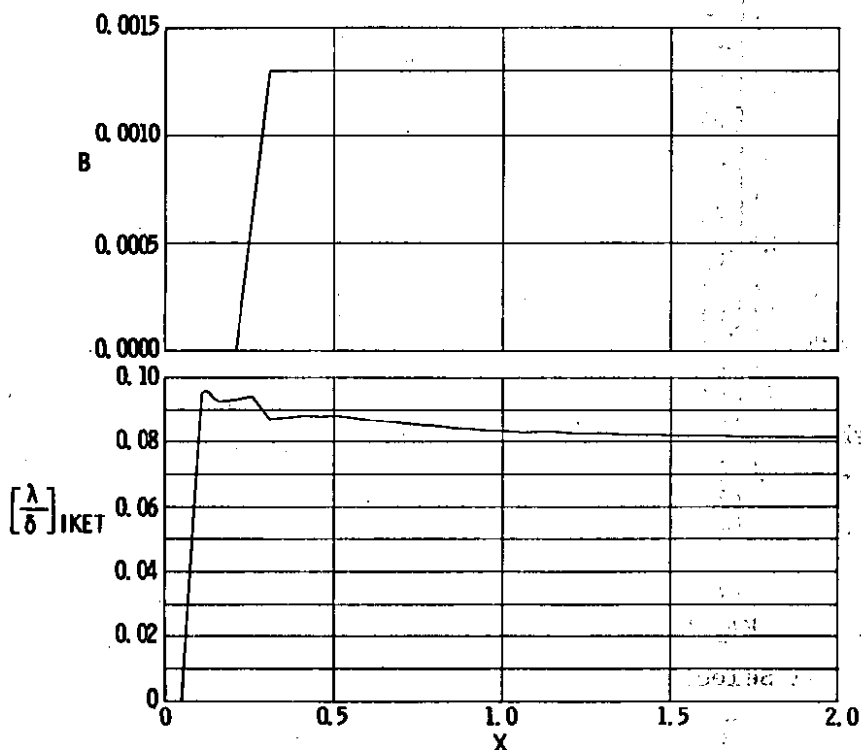
Figure 32. B and $[\lambda/\delta]_{IKET}$ for Squire's $M_\infty = 2.5$ case.

4.0 CONCLUSIONS

The IKET-based extended-mixing-length hypothesis as developed and assessed in this report has been demonstrated to be an effective technique for the calculation of many different compressible turbulent boundary-layer flows. The ability to calculate the outer-region length

scale for turbulent shear stress has been shown to be important for
flows with significant pressure gradients, roughness, and transpiration,
and necessary for flows undergoing transition and relaminarization. The
baseline turbulence model employed and the modifications made to the
baseline model embody a great deal of the "physics" of compressible
turbulent boundary-layer flows. For situations in which the applica-
bility of conventional mixing-length analyses is questionable or doubtful,
the extended mixing-length approach delineated in this report provides a
next logical degree of sophistication.

REFERENCES

1. Launder, B. E. and Spalding, D. B. Lectures in Mathematical
    Models of Turbulence. Academic Press, Inc., London and
    New York, 1972.

2. Bradshaw, P. "The Understanding and Prediction of Turbulent
    Flow." Aeronautical Journal, Vol. 76, No. 739, July 1972,
    pp. 403-418.

3. Harlow, F. H., Editor. "Turbulence Transport Modeling."
    AIAA Selected Reprint Series, Vol. XIV, February 1973.

4. Mellor, G. L. and Herring, H. J. "A Survey of Mean Turbulent
    Field Closure Models." AIAA Journal, Vol. 11, No. 5,
    May 1973, pp. 590-599.

5. Bradshaw, P. "The Strategy of Calculation Methods for Complex
    Turbulent Flows." Imperial College Aero Report 73-05,
    August 1973.

6. Launder, B. E. and Spalding, D. B. "The Numerical Computation of Turbulent Flows." Computer Methods in Applied Mechanics and Engineering, Vol. 3, No. 2, March 1974, pp. 269-289.

7. White, F. M. Viscous Fluid Flow. McGraw-Hill, Inc., New York, 1974.

8. Cebeci, T. and Smith, A.M.O. Analysis of Turbulent Boundary Layers. Academic Press, Inc., New York, 1974.

9. Bushnell, D. M., Cary, A. M., Jr., and Harris, J. E. "Calculation Methods for Compressible Turbulent Boundary Layers State-of-the-Art 1976." Presented at the von Kármán Institute for Fluid Dynamics Lecture Series 86, "Compressible Turbulent Boundary Layers," March 1976.

10. Patankar, S. V. and Spalding, D. B. Heat and Mass Transfer in Boundary Layers. CRC Press, Cleveland, Ohio, 1968.

11. McDonald, H. and Camarata, F. J. "An Extended Mixing Length Approach for Computing the Turbulent Boundary Layer Development." Proceedings Computation of Turbulent Boundary Layers - 1968 AFOSR-IFP-Stanford Conference, Vol. 1, Stanford University, Stanford, California, August 1968, pp. 83-98.

12. McDonald, H. and Fish, R. W. "Practical Calculations of Transitional Boundary Layers." International Journal of Heat and Mass Transfer, Vol. 16, No. 9, September 1973, pp. 1729-1744; also AGARD-AG-164, December 1972, pp. 29-53.

13. Shamroth, S. J. and McDonald, H. "Assessment of a Transitional Boundary Layer Theory at Low Hypersonic Mach Numbers." NASA CR-213, November 1972.

14. McDonald, H. and Kreskovsky, J. P. "Effect of Free Stream Turbulence on the Turbulent Boundary Layer." International Journal of Heat and Mass Transfer, Vol. 17, No. 7, July 1974, pp. 705-716.

15. Chan, Y. Y. "Comparison of Several Mixing Length Models for Turbulent Boundary-Layer Computations." National Research Council of Canada Aeronautical Report LR-531, March 1970.

16. Chan, Y. Y. "Turbulent Boundary-Layer Computations Based on an Extended Mixing Length Approach." AIAA Journal, Vol. 8, No. 10, October 1970, pp. 1873-1875.

17. Chan, Y. Y. "Compressible Turbulent Boundary Layer Computations Based on an Extended Mixing Length Approach." C.A.S.I. Transactions, Vol. 5, No. 1, March 1972, pp. 21-27.

18. Bradshaw, P., Ferriss, D. H., and Atwell, N. P. "Calculation of Boundary-Layer Development Using the Turbulent Energy Equation." Journal of Fluid Mechanics, Vol. 28, Pt. 3, May 1967, pp. 593-616.

19. Vaglio-Laurin, R. "Turbulent Heat Transfer on Blunt-Nosed Bodies in Two-Dimensional and General Three-Dimensional Hypersonic Flow." WADC Technical Note 58-301, September 1958; also in Journal of Aeronautical Sciences, Vol. 27, No. 1, January 1960, pp. 27-36.

20. Laster, M. L. "Inhomogeneous Two-Stream Turbulent Mixing Using the Turbulent Kinetic Energy Equation." AEDC-TR-70-134 (AD705578), May 1970.

21. Bradshaw, P. and Ferriss, D. H. "Calculation of Boundary-Layer Development Using the Turbulent Energy Equation: Compressible Flow on Adiabatic Walls." Journal of Fluid Mechanics, Vol. 46, Pt. 1, March 1971, pp. 83–110.

22. Kaplan, W. Advanced Calculus. Addison-Wesley, Inc., Reading, Massachusetts, 1952.

23. Cebeci, T. and Bradshaw, P. Momentum Transfer in Boundary Layers. McGraw-Hill, Inc., New York, 1977.

24. Wolfshtein, M. "The Velocity and Temperature Distribution in One-Dimensional Flow with Turbulence Augmentation and Pressure Gradient." International Journal of Heat and Mass Transfer, Vol. 12, No. 3, March 1969, pp. 301–318.

25. Townsend, A. A. "Equilibrium Layers and Wall Turbulence." Journal of Fluid Mechanics, Vol. 11, Pt. 1, August 1961, pp. 97–120.

26. Rose, W. C. and Murphy, J. D. "Ratio of Reynolds Shear Stress to Turbulence Kinetic Energy in a Boundary Layer." The Physics of Fluids, Vol. 16, No. 6, June 1973, pp. 935–937.

27. Morkovin, M. V. "Effects of Compressibility on Turbulent Flows." Mechanics of Turbulence, edited by Favre, Gordon, and Breach, Inc., New York 1964, pp. 367–380.

28. Van Driest, E. R. "On Turbulent Flow Near a Wall." Journal of Aeronautical Sciences, Vol. 23, No. 11, November 1956, pp. 1007-1011, 1036.

29. Kays, W. M. and Moffat, R. J. "The Behavior of Transpired Turbulent Boundary Layers." Studies in Convection: Theory, Measurement and Applications, Vol. 1, edited by B. E. Launder, Academic Press, Inc., New York, 1975, pp. 223-319.

30. Healzer, J. M., Moffat, R. J., and Kays, W. M. "The Turbulent Boundary Layer on a Porous Rough Plate: Experimental Heat Transfer with Uniform Blowing." AIAA Paper No. 74-680 and ASME Paper No. 74-HT-14, presented at the AIAA/ASME 1974 Thermophysics and Heat Transfer Conference, Boston, Massachusetts, July 15-17, 1974.

31. Horstman, C. C. "A Turbulence Model for Non-Equilibrium Adverse Pressure Gradient Flows." AIAA Paper No. 76-412, presented at the AIAA 9th Fluid and Plasma Dynamics Conference, San Diego, California, July 14-16, 1976.

32. Glowacki, W. J. and Chi, S. W. "A Study of the Effect of Pressure Gradient on the Eddy Viscosity and Mixing Length for Incompressible Equilibrium Turbulent Boundary Layers." NOLTR 74-105, May 1974.

33. Finson, M. L. "A Reynolds Stress Model for Boundary Layer Transition with Application to Rough Surfaces." AFOSR-TR-76-0322, August 1975.

34. Schlichting, H. Boundary Layer Theory. McGraw-Hill, Inc., New York, 1960 (Second Edition).

35. Furuya, Y., Miyata, M., and Fujita, H. "Turbulent Boundary Layer and Flow Resistance on Plates Roughened by Wires." Transactions of the ASME, Journal of Fluids Engineering, Vol. 98, Ser. 1, No. 4, December 1976, pp. 635-644.

36. Dirling, R. B., Jr. "A Method for Computing Roughwall Heat Transfer Rates on Reentry Nosetips." AIAA paper No. 73-763, presented at the AIAA 8th Thermophysics Conference, Palm Springs, Californiz, July 16-18, 1973.

37. Reda, D. C., Ketter, F. C., Jr., and Fan, C. "Compressible Turbulent Skin Friction on Rough and Rough/Wavy Walls in Adiabatic Flow." AIAA Paper No. 74-574, presented at the AIAA 7th Fluid and Plasma Dynamics Conference, Palo Alto, California, June 17-19, 1974.

38. Adams, J. C., Jr. "Implicit Finite-Difference Analysis of Compressible Laminar, Transitional and Turbulent Boundary Layers Along the Windward Streamline of a Sharp Cone at Incidence." AEDC-TR-71-235 (AD734535), December 1971.

39. Adams, J. C., Jr. "Numerical Calculation of the Subsonic and Transonic Turbulent Boundary Layer on an Infinite Yawed Airfoil." AEDC-TR-73-112 (AD763730), July 1973.

40. Conte, S. D. and de Boor, C. Elementary Numerical Analysis: An Algorithmic Approach. McGraw-Hill, Inc., New York, 1972 (Second Edition).

41. Householder, A. S. Principles of Numerical Analysis. Dover Publications, Inc., New York, 1974.

42. Klebanoff, P. S. "Characteristics of Turbulence in a Boundary Layer with Zero Pressure Gradient." NACA TN 3178, July 1954.

43. Squire, H. B. and Young, A. D. "The Calculation of the Profile Drag of Aerofoils." ARC R & M No. 1838, 1938.

44. Finson, M. L., Lewis, P. F., Wu, P.K.S., Teare, J. D., Pirri, A. N., and Nebolsine, P. E. "Advanced Reentry Aeromechanics." PSI TR-10, August 1974.

45. Nash-Webber, J. L. "Wall Shear-Stress and Laminarization in Accelerated Turbulent Compressible Boundary Layers." MIT Gas Turbine Lab. Report No. 94, April 1968.

46. Kreskovsky, J. P., Shamroth, S. J., and McDonald, H. "Parametric Study of Relaminarization of Turbulent Boundary Layers on Nozzle Walls." NASA CR-2370, June 1974.

47. Lewis, J. E., Gran, R. L., and Kubota, T. "An Experiment on the Adiabatic Compressible Turbulent Boundary Layer in Adverse and Favorable Pressure Gradients." Journal of Fluid Mechanics, Vol. 51, Pt. 4, February 1972, pp. 657-672.

48. Gran, R. L., Lewis, J. E., and Kubota, T. "The Effect of Wall Cooling on a Compressible Turbulent Boundary Layer." Journal of Fluid Mechanics, Vol. 66, Pt. 3, November 1974, pp. 507-528.

49. Hahn, J. S. and Lutz, R. "Experimental Investigation of Turbulent Boundary Layers with Pressure Gradient and Heat Transfer at Mach Number 4." AEDC-TR-71-3 (AD879136L), January 1971.

50. Johnson, C. B. and Kaufman, L. G. III. "Interference Heating from Interactions of Shock Waves with Turbulent Boundary Layers at Mach 6." NASA TN D-7649, September 1974.

51. Reeves, B. L. "A Two-Layer Model of High Speed Two- and Three-Dimensional Turbulent Boundary Layers with Pressure Gradient and Surface Mass Injection." SAMSO-TR-72-25, November 1971.

52. Bradshaw, P. "The Effect of Mean Compression or Dilatation on the Turbulence Structure of Supersonic Boundary Layers." Journal of Fluid Mechanics, Vol. 63, Pt. 3, April 1974, pp. 449-464.

53. Deem, R. E., Erickson, C. R., and Murphy, J. S. "Flat-Plate Boundary-Layer Transition at Hypersonic Speeds." FDL-TDR-64-129, October 1964.

54. Pate, S. R. and Schueler, C. J. "Radiated Aerodynamic Noise Effects on Boundary-Layer Transition in Supersonic and Hypersonic Wind Tunnels." AIAA Journal, Vol. 7, No. 3, March 1969, pp. 450-457.

55. Goldstein, M. E. Aeroacoustics. McGraw-Hill International Book Co., New York, 1976.

56. Laderman, A. J. "Hypersonic Viscous Flow over a Slender Cone. Part II: Turbulence Structure of a Boundary Layer." AIAA Paper No. 74-534, presented at the AIAA 7th Fluid and Plasma Dynamics Conference, Palo Alto, California, June 1974.

57. Reshotko, E. "Boundary Layer Stability and Transition." Annual Reviews of Fluid Mechanics, Vol. 8, Annual Reviews, Inc., Palo Alto, California, 1976, pp. 311-349.

58. Bushnell, D. M. and Alston, D. W. "Calculation of Transitional Boundary-Layer Flows." AIAA Journal, Vol. 11, No. 4, April 1973, pp. 554-556.

59. Potter, J. L. and Whitfield, J. D. "Effects of Slight Nose Bluntness and Roughness on Boundary-Layer Transition in Supersonic Flows." Journal of Fluid Mechanics, Vol. 12, Pt. 4, April 1962, pp. 501-535.

60. Stainback, P. C. "Use of Rouse's Stability Parameter in Determining the Critical Layer Height of a Laminar Boundary Layer." AIAA Journal, Vol. 8, No. 1, January 1970, pp. 173-175.

61. Fischer, M. C. and Weinstein, L. M. "Cone Transitional Boundary-Layer Structure at M_e = 14." AIAA Journal, Vol. 10, No. 5, May 1972, pp. 699-701.

62. Adams, J. C., Jr. "Eddy Viscosity-Intermittency Factor Approach to Numerical Calculation of Transitional Heating on Sharp Cones in Hypersonic Flow." AEDC-TR-70-210 (AD714058), November 1970.

63. Harris, J. E. "Numerical Solution of the Equations for Compressible Laminar, Transitional, and Turbulent Boundary Layers and Comparisons with Experimental Data." NASA TR R-368, August 1971.

64. Kuhn, G. D. "Calculation of Compressible, Nonadiabatic Boundary Layers in Laminar, Transitional, and Turbulent Flow by the Method of Integral Relations." NASA CR-1797, November 1971.

65. Mack, L. M. "Linear Stability Theory and the Problem of Supersonic Boundary-Layer Transition." AIAA Journal, Vol. 13, No. 3, March 1975, pp. 278-289.

66. Pate, S. R. "Measurements and Correlations of Transition Reynolds Numbers on Sharp Slender Cones at High Speeds." AIAA Paper No. 70-799, presented at AIAA 3rd Fluid and Plasma Dynamics Conference, Los Angeles, California, June 29-July 1, 1970; also AIAA Journal, Vol. 9, No. 6, June 1971, pp. 1082-1090.

67. Evans, M. R. "Boundary-Layer Integral Matrix Procedure Including Gas Phase Kinetics, KBLIMP-A." Aerotherm UM 75-62, March 1975.

68. Inouye, M., Rakich, J. V., and Lomax, H. "A Description of Numerical Methods and Computer Programs for Two-Dimensional and Axisymmetric Supersonic Flow over Blunt-Nosed and Flared Bodies." NASA TN D-2970, August 1965.

69. Aungier, R. H. "A Computational Method for Exact, Direct and Unified Solutions for Axisymmetric Flow over Blunt Bodies of Arbitrary Shape (Program BLUNT), " AFWL-TR-70-16, July 1970.

70. Bushnell, D. M., Cary, A. M., Jr., and Holley, B. B. "Mixing Length in Low Reynolds Number Compressible Turbulent Boundary Layers." AIAA Journal, Vol. 13, No. 8, August 1975, pp. 1119-1121.

71. Maise, G. and McDonald, H. "Mixing Length and Kinematic Eddy Viscosity in a Compressible Boundary Layer." AIAA Journal, Vol. 6, No. 1, January 1968, pp. 73-80.

72. Horstman, C. C. and Owen, F. K. "Turbulent Properties of a Compressible Boundary Layer." AIAA Journal, Vol. 10, No. 11, November 1972, pp. 1418-1424.

73. Squire, L. C. "Eddy Viscosity Distributions in Compressible Turbulent Boundary Layers with Injection." The Aeronautical Quarterly, Vol. 22, May 1971, pp. 169-182.

74. Squire, L. C. "Further Experimental Investigations of Compressible Turbulent Boundary Layers with Air Injection." ARC R & M No. 3627, August 1968.

75. Pletcher, R. H. "Prediction of Transpired Turbulent Boundary Layers." Transactions of the ASME, Journal of Heat Transfer, Vol. 96, Ser. C, No. 1, Febraury 1974, pp. 89-94.

76. Mellor, G. L. and Herring, H. J. "A Study of Turbulent Boundary Layer Models: Part II, Mean Turbulent Field Closure." SC-CR-70-6125B, January 1971.

77. Warsi, Z.U.A. and Mertaugh, L. J. "Estimation of Turbulent Energy Dissipation Using Available Transfer Theories." AIAA Journal, Vol. 12, No. 2, February 1974, pp. 237-239.

78. Hassid, S. and Poreh, M. "A Turbulent Energy Model for Flows with Drag Reduction." Transactions of the ASME, Journal of Fluids Engineering, Vol. 97, Ser. 1, No. 2, June 1975, pp. 234-241.

79. Jones, W. P. and Launder, B. E. "The Prediction of Laminarization with a Two-Equation Model of Turbulence." International Journal of Heat and Mass Transfer, Vol. 15, No. 2, February 1972, pp. 301-314.

80. Jones, W. P. and Launder, B. E. "The Calculation of Low-Reynolds-Number Phenomena with a Two-Equation Model of Turbulence." International Journal of Heat and Mass Transfer, Vol. 16, No. 6, June 1973, pp. 1119-1130.

APPENDIX A
DETERMINATION OF BASELINE TURBULENCE MODEL CONSTANTS

Classical turbulent boundary-layer theory, as well as recent experimental data, is used to deduce plausible values of the empirical constants in the turbulence model. The structural scales a_t (the fully turbulent value of the structural scale a_1), a_2, and a_3 are taken from Bradshaw, Ferriss, and Atwell (Ref. 18) and Mellor and Herring (Ref. 76):

$$a_t = 0.150 \qquad\qquad (A-1)$$

$$a_2 = 0.566 \qquad\qquad (A-2)$$

$$a_3 = 0.150 \qquad\qquad (A-3)$$

Rose and Murphy (Ref. 26) concur with the value of Bradshaw et al. for a_t and further suggest that the probable validity of Morkovin's hypothesis is the reason why values of the structural scales based upon incompressible flow data may be used for compressible flows. It is further assumed that the a_2 and a_3 scales remain constant across the entire boundary layer.

The empirical constant C_μ is deduced by equating the classical mixing-length expression for μ_t in the inner region but outside of the viscous sublayer,

$$\mu_t = \bar{\rho} \, \kappa^2 \, y^2 \, \partial\bar{u}/\partial y \qquad\qquad (A-4)$$

[where κ is the von Kármán constant taken to have in the baseline turbulence model the value of 0.435 (Ref. 10)] with the equivalent expression for the Wolfshtein (Ref. 24) model used in this paper:

$$\mu_t = \left(C_\mu^2/2a_t\right) \bar{\rho} \, y^2 \, \partial\bar{u}/\partial y \qquad\qquad (A-5)$$

(where the structural scale a_1 has been set equal to the fully turbulent value a_t since Eq. (A-5) is applicable outside the viscous sublayer) and thus, using the previously defined values of a_t and κ, one finds that

$$C_\mu = \kappa\sqrt{2a_t} = 0.2383 \qquad\qquad (A-6)$$

The empirical constant C_D can be evaluated by neglecting all terms in the turbulent kinetic energy equation except production and dissipation. Turbulence production equaling turbulent dissipation is applicable only outside the viscous sublayer, where it is logical to assume ℓ_μ and ℓ_D also are equal. This is in essence a local equilibrium model of turbulence and represents the well-known mixing-length approach. From Eq. (13) with turbulence production equal to turbulence dissipation [see section IV of chapter II in the report by Laster (Ref. 20) ,

$$\tau_t \, \partial\overline{u}/\partial y = \overline{\rho} \, \epsilon \qquad\qquad (A-7)$$

which upon substitution of Eqs. (35) and (36) reduces to

$$\left(C_\mu^2/2a_t\right) \, \overline{\rho} \, \ell_\mu^2 \, (\partial\overline{u}/\partial y)^3 = \left(\frac{C_D\overline{\rho}}{\ell_D}\right) \left(\frac{C_\mu}{2a_t} \ell_\mu \frac{\partial\overline{u}}{\partial y}\right)^3 \qquad (A-8)$$

and which yields

$$C_D = (2a_t)^2/C_\mu = 0.3777 \qquad\qquad (A-9)$$

which is in reasonable agreement with the results of Warsi and Mertaugh (Ref. 77), who suggest a value of 0.4525.

The behavior of the inner region of the turbulent boundary layer is dependent upon the damping functions [Eqs. (41), (42), and (43)] of the length scales and the structural scale a_1 as given by Eqs. (38), (39), and (40). The constants A_μ, A_D, and A_a determine the behavior of the inner region damping.

The numerical value of A_μ was taken as recommended by Wolfshtein (Ref. 24), namely

$$A_\mu = 0.0160 \tag{A-10}$$

The value of A_μ is dependent upon the near-wall behavior of ℓ_μ and the dissipation of turbulent energy as discussed by Hassid and Poreh (Ref. 78).

The value of the empirical constant A_D is deduced using the limiting near-wall form of the turbulent kinetic energy equation given by Jones and Launder (Refs. 79 and 80),

$$\partial/\partial y \ [\bar{\mu} \ (\partial k/\partial y)] - \bar{\rho} \ \epsilon = 0 \tag{A-11}$$

Using the value of $\bar{\rho} \ \epsilon$ given in Eq. (24) and writing ℓ_D for small values of y as

$$\ell_D \approx A_D \ R_t \ y = A_D \ \frac{\bar{\rho} \ k^{1/2} \ y^2}{\bar{\mu}} \tag{A-12}$$

yields, when substituted in Eq. (A-11),

$$\bar{\mu} \ (\partial^2 k/\partial y^2) + (\partial\bar{\mu}/\partial y) \ (\partial k/\partial y) = (C_D/A_D) \ (\bar{\mu}k/y^2) \tag{A-13}$$

According to Jones and Launder, the turbulent kinetic energy in the near-wall region is quadratic in y; hence,

$$k = \alpha y^2, \ \alpha \text{ constant} \tag{A-14}$$

and Eq. (A-11) becomes

$$2\alpha\bar{\mu} + 2\alpha y \ (\partial\bar{\mu}/\partial y) = (C_D/A_D) \ (\alpha\bar{\mu}y^2/y^2) \tag{A-15}$$

Equation (A-15) when evaluated at the wall results in

$$A_D = C_D/2 = 0.18885 \qquad\qquad (A-16)$$

The evaluation of the empirical constant A_a is begun by writing the local turbulence Reynolds number as

$$R_t = \frac{\overset{\circ}{\rho}k^{1/2}y}{\overline{\mu}} = \frac{\overline{\rho}\sqrt{\tau_t/(2a_1\,\overline{\rho})}\;y}{\overline{\mu}} = \frac{y^+\sqrt{\tau_t/\tau_w}}{\sqrt{2a_1}} \qquad (A-17)$$

where

$$y^+ = \frac{\overline{\rho}\;\sqrt{\tau_w/\rho}\;y}{\overline{\mu}} \qquad\qquad (A-18)$$

and where Eq. (25) has been used to relate the turbulent kinetic energy to the turbulent shear stress. The local wall shear stress is denoted by τ_w. Squaring Eq. (A-17) and substituting Eqs. (40) and (43) for a_1 gives

$$R_t^2 = \frac{(y^+)^2\;(\tau_t/\tau_w)}{2a_t\left[1 - \exp(-A_a\,R_t)\right]} \qquad (A-19)$$

which in the near-wall region where R_t is small becomes

$$A_a\,R_t^3 \approx \frac{(y^+)^2\;(\tau_t/\tau_w)}{2a_t} \qquad\qquad (A-20)$$

Using the near-wall approximations

$$\ell_\mu \approx A_\mu R_t y \qquad\qquad (A-21)$$

$$a_1 \approx A_a R_t a_t \qquad\qquad (A-22)$$

in conjunction with the turbulent shear stress as defined by Eq. (35) results in

$$\tau_t \approx \frac{c_\mu^2}{2A_a R_t a_t} \quad \bar{\rho} \left(A_\mu R_t y \frac{\partial \bar{u}}{\partial y} \right)^2 \tag{A-23}$$

which is valid in the near-wall region. Equation (A-23) via use of the friction velocity

$$u^+ = \frac{\bar{u}}{u_w^+} \tag{A-24}$$

and y^+ as given in Eq. (A-18) can be arranged as

$$\tau_t/\tau_w = \left(c_\mu^2/2a_t \right) \left(A_\mu^2/A_a \right) R_t (y^+)^2 (\partial u^+/\partial y^+)^2 \tag{A-25}$$

In the near-wall region, the classical work of van Driest indicates that

$$\tau_t/\tau_w \approx \kappa^2 (y^+)^4/(A^+)^2 \tag{A-26}$$

$$\partial u^+/\partial y^+ \approx 1 - \kappa^2 (y^+)^4/(A^+)^2 \tag{A-27}$$

where A^+ is a numerical constant. Use of Eq. (A-26) in Eq. (A-20) gives

$$A_a R_t^3 = \frac{\kappa^2 (y^+)^6}{2a_t (A^+)^2} \tag{A-28}$$

whereas using Eqs. (A-26) and (A-27) in Eq. (A-25) results in

$$R_t = \frac{2a_t A_a}{A_\mu^2 c_\mu^2} \frac{\kappa^2(y^+)^2}{(A^+)^2 [1 - \kappa^2 (y^+)^4/(A^+)^2]^2} \tag{A-29}$$

The expression R_t as given in the above equation allows Eq. (A-20) to be written in terms of A_a as

$$A_a^4 = \frac{\left(A_\mu \, C_\mu \, A^+\right)^6 \left[1 - \kappa^2 (y^+)^4/(A^+)^2\right]^6}{\left[2a_t \, \kappa^2 \, (y^+)^2\right]^3} \quad \frac{\kappa^2 (y^+)^6}{2a_t (A^+)^2} \qquad \text{(A-30)}$$

which when evaluated at the wall reduces to

$$A_a = (A^+/2a_t\kappa) \, (A_\mu \, C_\mu)^{3/2} = 0.0469 \qquad \text{(A-31)}$$

where A^+ is taken to have the value 26.0.

The last constant to be determined is λ_D. The classical mixing-length expression for the turbulent viscosity μ_t in the outer region is

$$\mu_t = \bar{\rho} \, \lambda^2 \, \delta^2 \, (\partial\bar{u}/\partial y) \qquad \text{(A-32)}$$

where λ is usually taken as 0.09. Assuming local equilibrium so that ℓ_μ and ℓ_D are equal permits the turbulent viscosity of Wolfshtein to be written as

$$\mu_t = (C_\mu^2 \, /2a_t) \, \bar{\rho} \, \lambda_D^2 \, \delta^2 \, (\partial\bar{u}/\partial y) \qquad \text{(A-33)}$$

Comparison of Eqs. (A-32) and (A-33) results in

$$\lambda_D = \sqrt{2a_t/C_\mu^2} \; \lambda = 0.2069 \qquad \text{(A-34)}$$

based on a value for λ of 0.09.

NOMENCLATURE

A_a — Damping constant for structural scale a_1

A_D — Damping constant for dissipation length scale

A_s — Roughness element windward surface area

A_p — Roughness element cross-sectional area

A^+ — van Driest damping constant, 26.0

A^+_{eff} — Effective damping constant for mixing length

A_μ — Damping constant for turbulence shear stress

a — Constant in Eq. (54)

a_1 — Structural scale given by Eq. (25)

a_2 — Structural scale given by Eq. (26)

a_3 — Structural scale given by Eq. (27)

a_t — Fully turbulent value of structural scale a_1

B — Blowing coefficient given by Eq. (77)

b — Constant in Eq. (54)

C_D — Dissipation constant used in Eq. (24)

C_{D_r} — Drag coefficient of roughness element

C_f Skin friction

C_μ Turbulent viscosity constant used in Eq. (23)

c Constant in Eq. (54)

c_p Constant pressure specific heat

D Turbulent kinetic energy dissipation

D_a Wall damping for structural scale a_1

D_D Wall damping for dissipation length scale

D_r Diameter of roughness element

D_μ Wall damping for turbulent shear stress

E Incident energy absorbed by boundary layer

$\bar{E}_e$ Dimensionless energy absorbed, $E/\rho_e U_e^3$

E_r Turbulent kinetic energy generation attributable to roughness

f Roughness model constant used in Eq. (63)

$\bar{h}$ Mean static enthalpy

H_{pk} Peak heating ratio in Eq. (76)

IKET   Integral kinetic energy of turbulence

j 1 for axisymmetric, 0 for two-dimensional

94

K　　　　Acceleration parameter given by Eq. (74)

k　　　　$1/2\left[\overline{(u')^2} + \overline{(v')^2} + \overline{(w')^2}\right]$

k_a　　　Roughness element height, actual

k_r　　　Roughness element height, sand grain equivalent

k_t　　　Turbulent thermal conductivity

ℓ　　　Tensor index in Eq. (14)

ℓ_D　　　Length scale for dissipation

ℓ_r　　　Center-to-center roughness element spacing

ℓ_μ　　　Length scale for turbulent shear stress

M　　　　Mach number

M_e　　　Edge Mach number

m　　　　Tensor index in Eq. (14)

n　　　　Exponent in Eq. (73), 0.85

P_{pk}　　　Peak heating ratio in Eq. (76)

Pr　　　Laminar Prandtl number, 0.71

Pr_t　　　Turbulent Prandtl number, 0.90

p'　　　Fluctuating pressure

95

$\bar{p}$ Mean pressure

p^{+} Dimensionless pressure gradient

$\overline{p^{+}(x)}$ Weighed pressure gradient given by Eq. (55)

Q_u Constant in Eq. (66), 0.1

$\dot{q}$ Heat-transfer rate

$\dot{q}_o$ Heat-transfer rate at stagnation point

$\overline{q^2}$ $\overline{(u')^2} + \overline{(v')^2} + \overline{(w')^2}$

R Gas constant

R_N Nose radius

Re Reynolds number

Re_{e,x_t} Edge Reynolds number at transition

$Re_{e,\theta}$ Edge Reynolds number based on momentum thickness

$Re_{\infty}/in.$ Free-stream Reynolds number per inch

R_t Turbulent Reynolds number, $\bar{\rho} k^{\frac{1}{2}} y / \bar{\mu}$

R_{τ} Roughness Reynolds number, $u_w^{+} k_r / \nu_w$

r Radius for axisymmetric flow

St_{∞} Stanton number based on free-stream conditions and $(T_{o,\infty} - T_w)$

T   Temperature

$\bar{\bar{T}}$ Mean temperature

U_e Outer-edge velocity

$\bar{u}$ Mean streamwise velocity in boundary layer

u_∞ Free-stream velocity

u' Fluctuating streamwise velocity

u^+ Friction velocity, $\bar{u}/u_w^+$

u_w^+ Wall friction velocity, $\sqrt{\tau_w/\bar{\rho}_w}$

V   Velocity expression given by Eq. (5)

$\bar{v}$ Mean surface normal velocity in boundary layer

v' Fluctuating normal velocity

v_w^+ Dimensionless normal velocity at wall

w' Fluctuating lateral velocity

x   Streamwise coordinate

x_t Transition location

x_1 Initial point of laminar flow breakdown

x_2 Initial location of turbulent burst

97

Y   Outer-region length scale for turbulent shear stress

y   Normal coordinate

y_{cr} Location of maximum turbulent shear stress

y^+ Dimensionless normal coordinate given by Eq. (A-18)

α Constant used in Eq. (A-14)

β Dimensionless pressure gradient, $\delta_1^*(d\bar{p}/dx)/\tau_w$

$\bar{\beta}$ Weighed dimensionless pressure gradient given by Eq. (59)

γ Ratio of specific heats

δ Boundary-layer thickness

δ^* Boundary-layer displacement thickness

δ_1^* Kinematic displacement thickness

δy Infinitesimal length in coordinate y

ϵ $D/\bar{\rho}$ given in Eq. (23)

ζ Variable of integration in Eq. (55)

θ Boundary-layer momentum thickness

κ von Kármán constant

Λ Roughness element geometry parameter, $\ell_r/k_a (As/Ap)^{4/3}$

λ Conventional outer-region parameter in Eq. (A-32)

λ_D Outer-region empirical constant in Eq. (46)

λ_ℓ Lag length parameter used in Eq. (55)

$\bar{\mu}$ Mean molecular viscosity

μ_t Turbulent viscosity given by Eq. (22)

$\bar{\nu}$ Mean molecular kinematic viscosity

$\bar{\rho}$ Mean density

ρ' Fluctuating density

σ Lag parameter defined by Eq. (57)

$\sigma'_{\ell m}$ Shear stress tensor

τ Shear stress

ω Expression given by Eq. (56)

SUBSCRIPTS

e   Outer edge of boundary layer

o, ∞ Free-stream stagnation

r   Roughness

t   Turbulent

w   Wall

∞   Free-stream

SUPERSCRIPTS

´   Fluctuation quantity

—   Quantity averaged with respect to time